NASA Contractor Report 186034

A Concept for Adaptive Performance Optimization on Commercial Transport Aircraft

Michael R. Jackson and Dale F. Enns

NASA Contract NAS4-50021
September 1995

National Aeronautics and
Space Administration

NASA Contractor Report 186034

A Concept for Adaptive Performance Optimization on Commercial Transport Aircraft

Michael R. Jackson
and Dale F. Enns
Honeywell Technology Center
Minneapolis, Minnesota

Prepared for
NASA Dryden Flight Research Center
Edwards, California
Under Contract NAS4-50021

1995

National Aeronautics and
Space Administration

Dryden Flight Research Center
Edwards, California 93523-0273

Contents

List of Figures

Chapter 1

Introduction

Increasing competition among airline manufacturers and operators has highlighted the issue of aircraft efficiency. Manufacturers view increased operating efficiency as a means to attract and retain customers in an overall shrinking market. Airlines view increased efficiency as essential to minimizing fuel costs and lowering the 'break-even' operating point.

One means to improve aircraft operating efficiency is to exploit the redundant control effector capability present in all commercial transport aircraft. This means that there exists more than one means of trimming out the forces and moments required to obtain any desired steady-state flight condition. This additional freedom can be used to achieve drag reduction capabilities. Currently, aircraft flight conditions are fine-tuned through thousands of hours of wind tunnel and flight testing to 'optimize' the aerodynamic configuration. The resulting configuration is a compromise between cruise performance and low speed performance. True aircraft performance optimization is a highly integrated problem which requires state-of-the-art controls technology to optimize the performance of an integrated aircraft including both aerodynamic and propulsive disciplines.

Most aircraft have a Flight Management System (FMS) which produces model-based (predicted) optimal trajectories that define the altitude and velocity paths the aircraft follows. It is envisioned that a first cut adaptive performance optimization system would minimize drag at the FMS-determined flight conditions. Future efforts could investigate global optimization of the flight condition and redundant surface positions.

This report documents an adaptive control approach developed by Honeywell Technology Center for minimizing trim drag, along a specified trajectory, for subsonic transport aircraft. This approach is based on an on-line least squares estimation method used to develop a model of the aerodynamic effects of the redundant surfaces. This model is used to determine the optimal position of the redundant surfaces for the actual flight conditions experienced. The results are demonstrated through simulation studies using a simulation model of the

Lockheed L-1011 commercial transport aircraft. Although this particular report deals only with aerodynamic control surfaces, the approach is equally applicable to engines with redundant control capability.

1.1 Problem Statement

This objectives of the study described in this report are as follows.

1. Quantify the relationship between the excitation signal parameters and the performance of the adaptive controller during steady level flight using the active ailerons.
2. Extend the approach to simultaneously optimize the active ailerons (symmetric deflection of ailerons) and the outboard flaps during steady level flight.
3. Extend the approach to optimize the active ailerons during a climbing trajectory with a fixed throttle, following a given calibrated airspeed until the cruise Mach is obtained, then continuing to climb holding the cruise Mach number.

1.2 Terminology

The term "redundant surface" will often be used in this report to refer specifically to the additional surfaces that are available for optimization. The horizontal tail surface is considered the primary pitch control effector, and the active ailerons and outboard flaps are considered to be the "redundant surfaces" and will be explicitly optimized. The steady state position of the primary control surface is implicitly optimized by ensuring that the aircraft is in trim while the redundant surfaces are optimized.

The term "redundant" is sometimes used to collectively refer to the set of all pitch control effectors as a "redundant set," where there is one constraint on the set (moment equilibrium) and the additional degrees of freedom can be used to optimize the set. However, this terminology is not used in this report.

1.3 Nomenclature

a	Speed of sound (ft/sec)
A	Excitation amplitude (deg)
$\bar{c}$	Mean aerodynamic chord (feet)
$\hat{c}$	Least squares solution
C_D	Drag coefficient
C_L	Lift coefficient
C_M	Pitching moment coefficient
E	Specific energy $(\text{ft/sec})^2$
h	Altitude (feet)
p	Ambient air pressure
PLA	Power lever angle (percent)
$\bar{q}$	Dynamic pressure (lb/ft^2)
q	Pitch rate (rad/sec)
s	Laplace variable
S	Wing area (sq. feet)
T	Thrust (lb)
u	Control signal vector
u_o	Effective control surface used for pitch axis autopilot feedback. Primarily δ_{ht}.
u_1	First effective control surface used for optimization. Primarily δ_{aa}.
u_2	Second effective control surface used for optimization. Primarily δ_{fl}.
V_t	True airspeed (ft/sec)
V_{CAS}	Calibrated airspeed (ft/sec)
α	Angle of attack (deg or rad)
δ_{ht}	Horizontal tail surface deflection (deg)
δ_{aa}	Active (symmetric) aileron deflection (deg)
δ_{fl}	Outboard flap deflection (deg)
γ	Flight path angle (deg or rad)
ρ	Air density $(slug/ft^3)$
ω	Excitation signal frequency (rad/sec)

Chapter 2

Modeling

The model used in the evaluation of the adaptive controller is the Lockheed L-1011. The Fortran simulation of the L-1011 at Dryden was loaded onto the computers at Honeywell, and the subroutines relating to the aerodynamics were incorporated into an existing Honeywell aircraft simulation. This simulation is an implementation of the full 6-degree-of-freedom rigid body equations of motion of an aircraft.

The model includes the following surfaces: horizontal tail, elevator, outboard and inboard ailerons, active ailerons (symmetric deflection of outboard ailerons), outboard and inboard flaps, and rudder. The horizontal tail surface is used as the primary pitch control surface, and the elevator is operated on a schedule based on the horizontal tail surface.

The vehicle weight used for all of the simulations in this report is 408,000 pounds. This weight does not change with time – fuel burn is not simulated.

2.1 Full Aerodynamic Model

The aerodynamic model is broken into two parts, a high-speed model that includes Mach effects, and a low-speed model that includes flap effects. The aerodynamic force and moment coefficients are functions of the surface positions, angle of attack, Mach number and vehicle mass properties. These functions are primarily implemented with data table lookups for components of the coefficients due to the independent variables.

The full aerodynamic model includes lift, pitching moment and drag due to the active ailerons, but the drag effects modeled are only linear. A quadratic drag term was added to the existing model, resulting in the following model for drag due to active outboard aileron

deflection:

$$C_{D_{\delta_{aa}}} = -0.0003\ \delta_{aa} + 0.0000375\ \alpha\ \delta_{aa} + 0.0001\ \delta_{aa}^2$$

where, δ_{aa} and α are measured in degrees.

The full aerodynamic model includes no flap effects at high speed. To obtain a model of the aerodynamics of small flap deflections at high speed, the lift and moment characteristics were assumed to be similar to the low speed model. A linear model of the lift and moment due to the flaps was developed at low speed using a least squares approach, and these aerodynamic coefficients were assumed to be valid for small deflections of the flaps at high speed. The drag model at low speeds is not useful for the purposes of small angle deflections, since the model only contains data points at ten degree intervals. The drag model for the outboard flaps at high speed was assumed to be similar to the outboard ailerons, and a simple model was formulated. The resulting aerodynamic model for the outboard flaps at high speeds is as follows:

$$C_{L_{\delta_{fl}}} = 0.001892\ \delta_{fl} \tag{2.1}$$

$$C_{M_{\delta_{fl}}} = -0.001365\ \delta_{fl} \tag{2.2}$$

$$C_{D_{\delta_{fl}}} = -0.0004\ \delta_{fl} + 0.0000375\ \alpha\ \delta_{fl} + 0.0002\ \delta_{fl}^2 \tag{2.3}$$

where, δ_{fl} and α are measured in degrees.

It is appropriate to stress that these models are not intended to be an accurate representation of the performance of the L-1011. Our intention is to create a model that is representative of the character of the actual model. This model will allow the testing of the adaptive controllers described in this report. Conclusions based on this report should be limited to the operation of the controllers to locate the optimum surface positions, and not on the size of the performance benefits to be gained by the use of the controllers.

2.2 Least Squares Approximate Aerodynamic Model

Some of the control algorithms described in this report require knowledge of the aircraft's aerodynamics. It is not practical to implement a large database, such as the L-1011 model described above, in a flight control computer. A special aerodynamic model is proposed and the coefficients of the model are determined using a least squares approach.

The special aerodynamic model is:

$$C_D = C_{D_1} + C_{D_2}\alpha + C_{D_3}\delta_{ht} + C_{D_4}\delta_{aa} + C_{D_5}\delta_{fl} + C_{D_6}\alpha^2 + C_{D_7}\delta_{ht}^2 + C_{D_8}\delta_{aa}^2 +$$

$$C_{D_9}\delta_{fl}^2 + C_{D_{10}}\alpha\delta_{ht} + C_{D_{11}}\alpha\delta_{aa} + C_{D_{12}}\alpha\delta_{fl}$$

$$C_L = C_{L_o} + C_{L_\alpha}\alpha + C_{L_{ht}}\delta_{ht} + C_{L_{aa}}\delta_{aa} + C_{L_{fl}}\delta_{fl} + C_{L_q}\frac{q\bar{c}}{2V_t}$$

$$C_M = C_{M_o} + C_{M_\alpha}\alpha + C_{M_{ht}}\delta_{ht} + C_{M_{aa}}\delta_{aa} + C_{M_{fl}}\delta_{fl} + C_{M_q}\frac{q\bar{c}}{2V_t}$$

The coefficients are assumed to be functions of Mach number only. The least squares estimate of the coefficients was computed for a series of flight conditions by calling the full aerodynamic database with a range of independent variables as described below.

Variable	Minimum	Maximum	Units	# Points
α	0	5	degrees	11
δ_{ht}	-6	0	degrees	4
δ_{aa}	-4	12	degrees	9
δ_{fl}	0	5	degrees	3

A least squares estimate of the aerodynamic coefficients was computed for 6 representative flight conditions. The results are summarized in the table below.

	M = 0.35	0.5	0.6	0.7	0.8	0.85	Units
C_{D_1}	0.01652	0.01541	0.01582	0.01596	0.01680	0.01783	no units
C_{D_2}	-.0003620	.00002116	-.0002090	-.0004786	-0.002206	-0.002267	per deg
C_{D_3}	-.0002477	-.0000459	-.0000927	-.0001339	-.0004517	-.0006368	per deg
C_{D_4}	-0.0003	-0.0003	-0.0003	-0.0003	-0.0003	-0.0003	per deg
C_{D_5}	-0.0004	-0.0004	-0.0004	-0.0004	-0.0004	-0.0004	per deg
C_{D_6}	.0006369	0.0004644	.0005637	.0006913	0.001551	0.003031	per deg^2
C_{D_7}	.0000090	.00001679	.00002096	.00002986	.00007727	.0001065	per deg^2
C_{D_8}	0.0001	0.0001	0.0001	0.0001	0.0001	0.0001	per deg^2
C_{D_9}	0.0002	0.0002	0.0002	0.0002	0.0002	0.0002	per deg^2
$C_{D_{10}}$	.0002766	0.0002326	0.0002791	0.0003436	0.0007318	0.001348	per deg^2
$C_{D_{11}}$	.0000375	0.0000375	0.0000375	0.0000375	0.0000375	0.0000375	per deg^2
$C_{D_{12}}$	.0000375	0.0000375	0.0000375	0.0000375	0.0000375	0.0000375	per deg^2
C_{L_o}	0.04853	0.06334	0.06209	0.06094	0.06292	0.06507	no units
C_{L_α}	0.09982	0.09496	0.1000	0.1051	0.1171	0.1297	per deg
$C_{L_{ht}}$	0.02299	0.02394	0.02497	0.02593	0.02622	0.02623	per deg
$C_{L_{aa}}$	0.002639	0.002460	0.002355	0.002269	0.002056	0.001727	per deg
$C_{L_{fl}}$	0.001892	0.001892	0.001892	0.001892	0.001892	0.001892	per deg
C_{M_o}	-0.07704	-0.08237	-0.08637	-0.09068	-0.09069	-0.09242	no units
C_{M_α}	-0.02427	-0.02218	-0.02274	-0.02328	-0.02460	-0.02456	per deg
$C_{M_{ht}}$	-0.05677	-0.05912	-0.06165	-0.06402	-0.06475	-0.06478	per deg
$C_{M_{aa}}$	-0.002824	-0.002966	-0.002975	-0.002913	-0.002751	-0.002515	per deg
$C_{M_{fl}}$	-0.001365	-0.001365	-0.001365	-0.001365	-0.001365	-0.001365	per deg

For a given flight condition, the above table is interpolated to the current Mach number to compute the aerodynamic coefficients.

The aerodynamic coefficients C_{M_q} and C_{L_q} were taken directly from the full aerodynamic model.

This least squares aerodynamic model is used in the guidance law, the inner loop control law, and the adaptive algorithm for optimization during climb. An analytical method to minimize drag using the least squares model will be presented in Appendix B.

2.3 Engine Model

A simple engine model was implemented for this study, since the detailed dynamical performance of the engine will not affect the results. The engine thrust is modeled by a first order lag on the throttle command, with a gain proportional to the density ratio, the throttle, and the rated sea level thrust. The rated sea level thrust for the L-1011 is 150,000 pounds.

$$T = T_{sl}\frac{\delta_{PLA}}{100}\left(\frac{\rho(h)}{\rho_{sl}}\right)\left(\frac{5}{s+5}\right)$$

This approximation of thrust variation with altitude is a standard approximation for turbojet and turbofan engines. (For example, see reference [5], page 499).

2.4 Sensor and Actuator Dynamics

The sensors and actuators are modeled by first order lags with the break frequencies summarized in Tables 2.1 and 2.2. The sensor models are very simplified, and pessimistic with respect to the speed of response. This does not have significant impact on the performance of the adaptive controller – especially since these signals are subsequently passed through even slower lag filters prior to use by the adaptive controller.

The simulation uses an angle-of-attack sensor for the altitude hold guidance algorithms and the inner loop control. It is recognized that typical autopilots do not use an α sensor. The closed loop characteristics of the guidance and control laws used in this report are similar to typical autopilots. The α sensor is not used by the adaptive controller.

Sensor	Bandwidth (rad/sec)
V_t	20
α	20
q	20
γ	20
h	20
$\bar{q}$	20
$\dot{V}_t$	20

Table 2.1: Sensor bandwidths used in simulation

Actuator	Bandwidth (rad/sec)
δ_{ht}	30
δ_{el}	30
δ_{aa}	30
δ_{PLA}	5
δ_{fl}	10

Table 2.2: Actuator bandwidths used in simulation

2.5 True Optimization of Aerodynamic Model

The true optimal position of the surfaces for the full aerodynamic model will be used to measure the performance of the adaptive algorithm. The true optimum was found by trimming the aircraft across a range of the redundant surfaces. The drag is plotted versus δ_{aa}, with $\delta_{fl} = 0$, in Figure 2.1. The drag is plotted versus δ_{aa} for various positions of δ_{fl} in Figure 2.2. The drag is plotted versus δ_{fl} for various positions of δ_{aa} in Figure 2.3. These plots were computed at the steady level flight condition of Mach = 0.827 (V_t = 803.5 ft/sec), altitude = 37,000 feet. Figure 2.4 shows the drag versus δ_{aa} at several points during the climb trajectory.

The optimal surface positions, the minimum drag points in the Figures shown, are summarized in Table 2.3. Where applicable, the flight conditions are related to the climb trajectory for cross reference to the climb simulations described in Section 5.5.

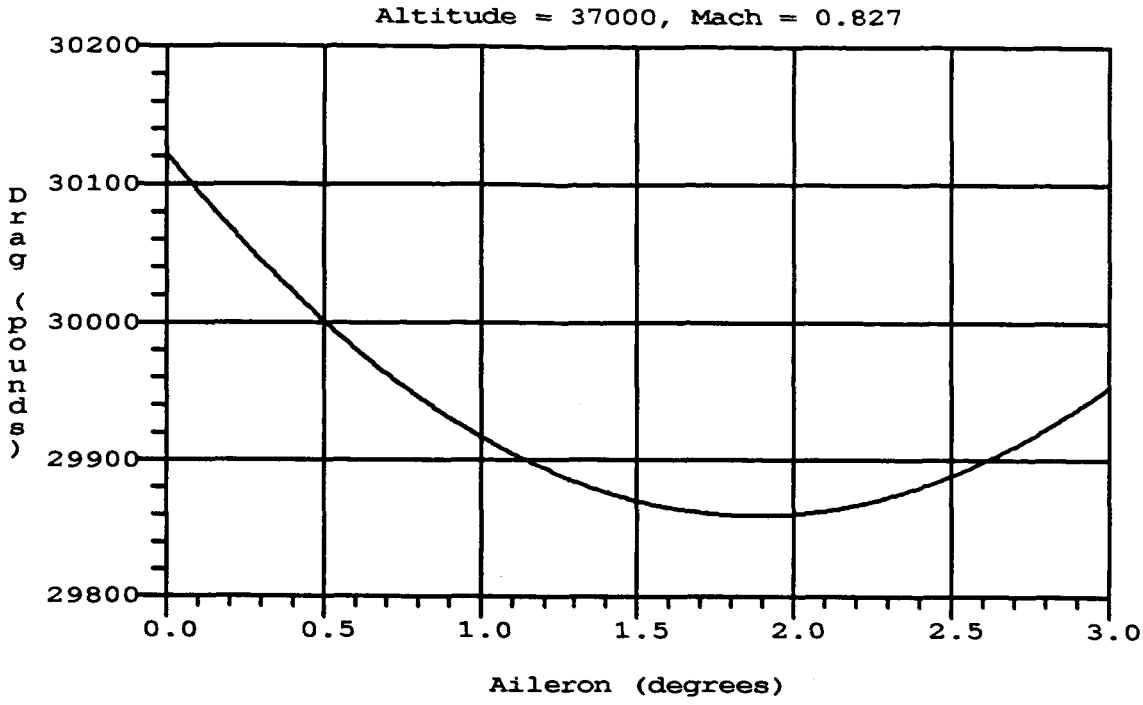

Figure 2.1: Trim Drag as a Function of Active Aileron

Altitude (feet)	Mach	Aileron (deg)	Flap (deg)	Trim Drag (pounds)	Time During Climb (sec)
10,000	0.576	0.0827	0	29000	0
18,000	0.670	0.511	0	29330	250
24,000	0.745	0.895	0	29530	600
29,000	0.820	1.241	0	29670	1100
33,000	0.820	1.549	0	29760	N/A
36,000	0.820	1.805	0	29831	N/A
37,000	0.827	1.880	0	29860	N/A
37,000	0.827	1.872	1.203	29640	N/A

Table 2.3: Minimum Drag as a Function of Altitude and Mach

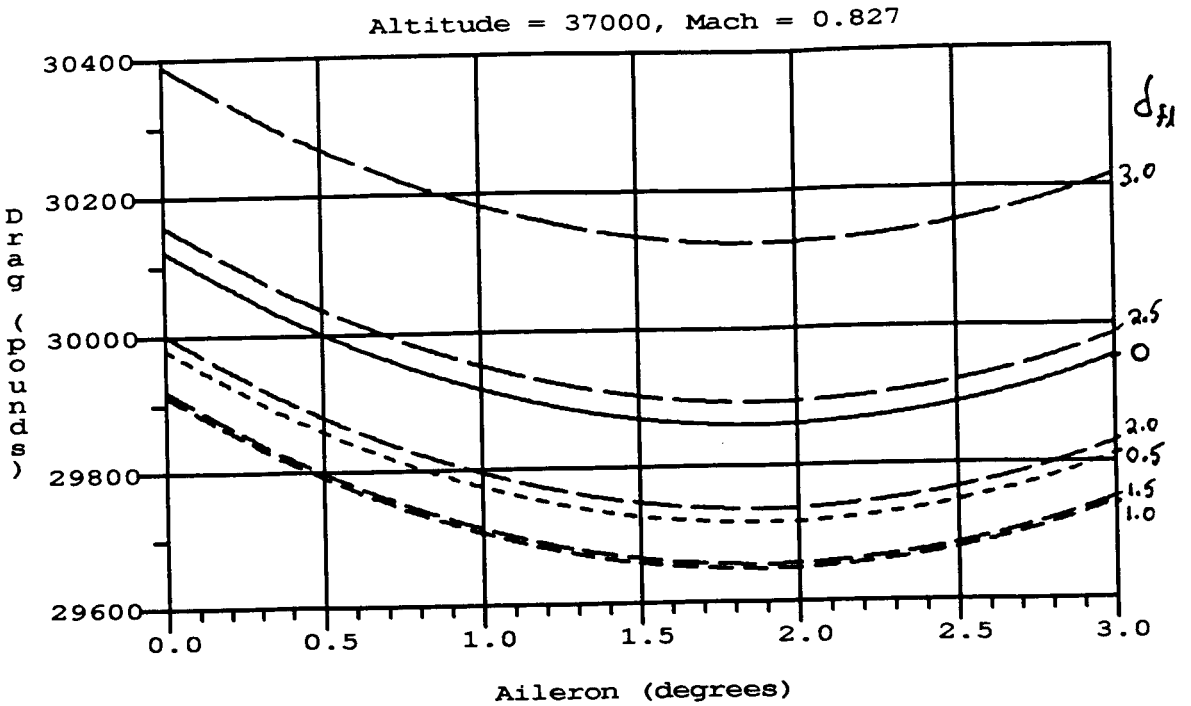

Figure 2.2: Trim Drag as a Function of Aileron for Various Flaps

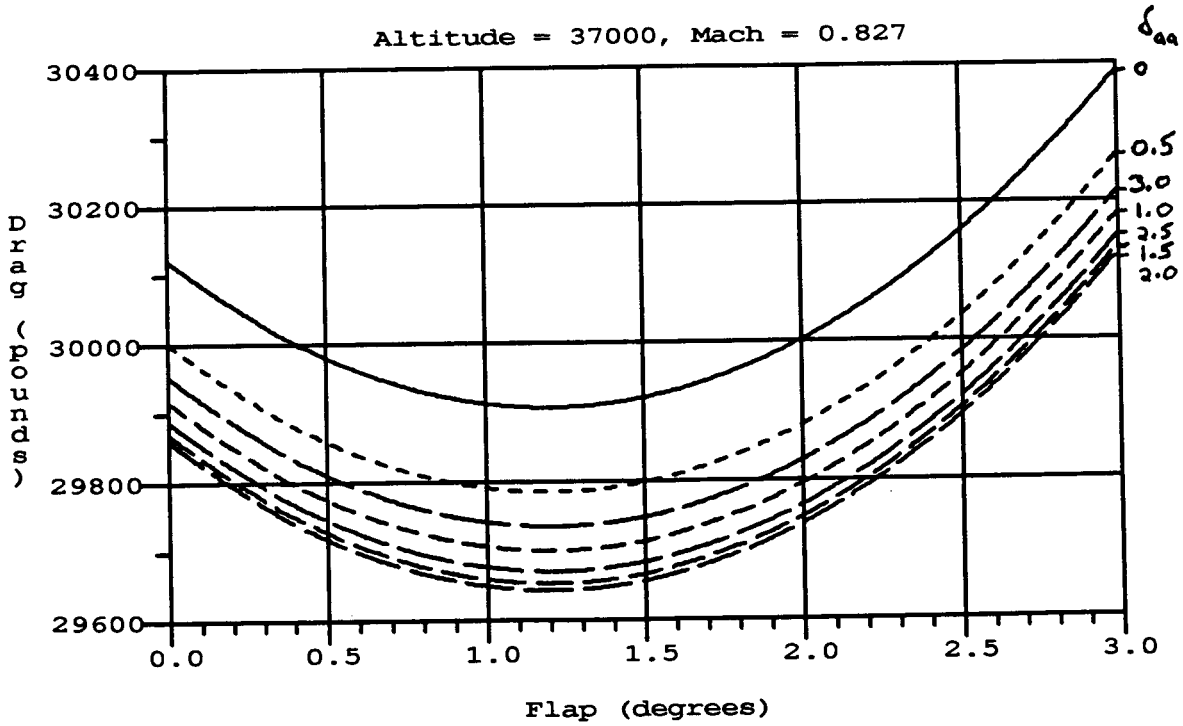

Figure 2.3: Trim Drag as a Function of Flap for Various Ailerons

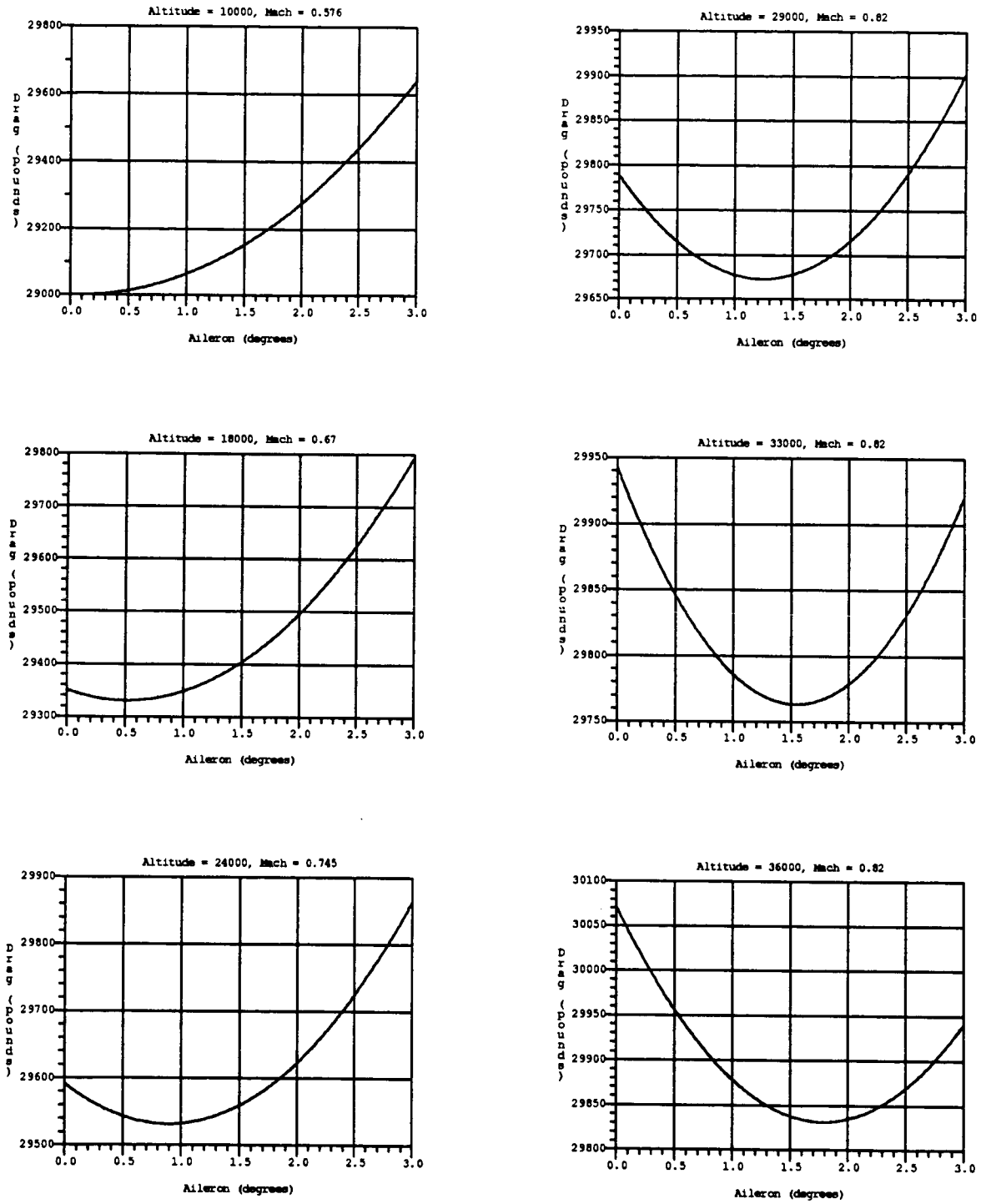

Figure 2.4: Trim Drag as a Function of Aileron, Altitude, Mach During Climb

Chapter 3

Feedback Optimization Approach

The approach used to optimize the redundant surface positions is based on a least squares estimation (LSE) algorithm to determine a model of the performance criterion as a function of the redundant surface positions. The redundant surfaces are excited by sinusoidal deflections to provide the LSE algorithm with sufficient information to compute a model. The model formed by the LSE is used to compute the surface positions that optimize the performance criteria.

This approach is based on the assumption that the aircraft is following altitude and velocity commands with the altitude and velocity loops closed via feedback.

Two performance criteria, or cost functions, were used in this report:

1. Thrust Command (T_c) was used for the steady level flight conditions.
2. Measured energy rate minus modeled energy rate ($\Delta\dot{E}$) was used for optimization during climb.

The performance criterion is denoted as J.

The true objective for the optimization during cruise is to minimize the fuel flow at a fixed airspeed, but a minimization of the commanded thrust will accomplish the same goal and does not require a model of the fuel flows.

The energy rate was selected as the performance criterion during climb instead of simply the rate of climb, since the energy rate will be less sensitive to disturbances than the climb rate. This will be discussed further in Section 3.3.

Figure 3.1 shows a general block diagram of the adaptive control method used in this report.

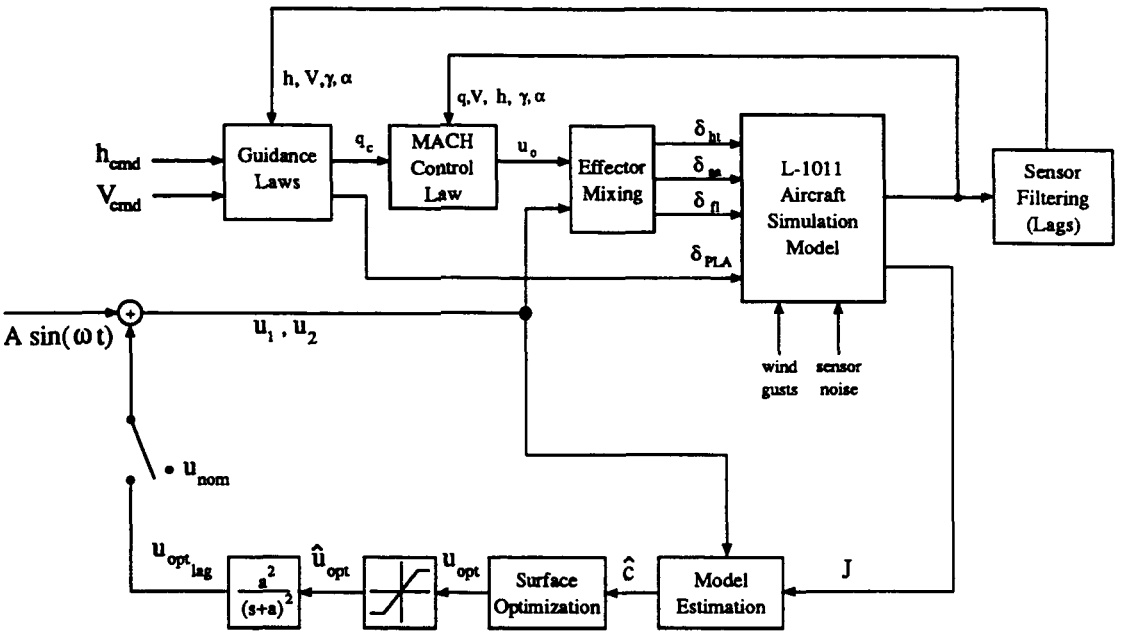

Figure 3.1: Block Diagram of Adaptive Control Method

3.1 Estimation Method

The model to be estimated is the performance criterion as a function of the redundant control surfaces, or $J(u)$. Both of the performance criteria used in this study depend directly on the drag due to the redundant surfaces, which is a parabolic function of the control surfaces.

3.1.1 Estimation for One Redundant Surface

Consider a model for one redundant control surface of the form:

$$J(u) = c_o + c_1 u_1 + c_2 u_1^2$$

where J represents the performance criterion and u_1 represents the redundant surface deflection. The objective of the estimation algorithm is to observe the measurements of the performance criterion J and correlate it with u_1.

A least squares algorithm can be used to fit many measured data points to the simplified model. Representing the measured data points in matrix form:

$$\begin{bmatrix} J_1 \\ J_2 \\ J_3 \\ . \\ . \end{bmatrix} = \begin{bmatrix} 1 & u_{1_1} & u_{1_1}^2 \\ 1 & u_{1_2} & u_{1_2}^2 \\ 1 & u_{1_3} & u_{1_3}^2 \\ . & . & . \\ . & . & . \end{bmatrix} \begin{bmatrix} c_o \\ c_1 \\ c_2 \end{bmatrix}$$

Representing the above matrix and vectors as A, b, and c:

$$b = Ac$$

A batch approach to a least squares solution can be found from the above equation alone, but it is undesirable to store this much information in the on-board computer and subsequently perform a batch solution. Typical batch solutions to least squares problems involve either a singular value decomposition of the A matrix, or an LU decomposition. The number of data points taken during the observation period is large (5,000 to 50,000), since the sensors are sampled often to allow the random disturbance effects to average out. Storage of this much data on a flight computer is not necessarily impractical, but it is unnecessary. The least squares solution will need to be computed periodically to determine when the model has converged, and computing a batch least squares solution on this large amount of data will be time consuming.

An alternative but equivalent approach to least squares solution is found by premultiplying both sides of the above equation by A^T to obtain the least squares solution $\hat{c}$.

$$(A^T A)\hat{c} = A^T b$$

This approach lends itself to onboard computation since the matrix $A^T A$ and the vector $A^T b$ can be generated real-time as summations of measurements. Written out fully:

$$\begin{bmatrix} \sum 1 & \sum u_1 & \sum u_1^2 \\ \sum u_1 & \sum u_1^2 & \sum u_1^3 \\ \sum u_1^2 & \sum u_1^3 & \sum u_1^4 \end{bmatrix} \begin{bmatrix} c_o \\ c_1 \\ c_2 \end{bmatrix} = \begin{bmatrix} \sum J \\ \sum u_1 J \\ \sum u_1^2 J \end{bmatrix}$$

Expressed in matrix form:

$$M\,\hat{c} = R \qquad \text{where } M = A^T A\,,\ R = A^T b$$

Each term in M and R can be computed on-line, adding the proper products of the current measurements of the control surface and cost function. The solution to the above equation can be found explicitly using matrix inversion, which is practical for a 3x3 matrix, or using an algorithm for solving simultaneous linear equations. The computations simplify greatly due to the symmetry of the matrix.

If the estimation algorithm is to be operating for short periods of time, the above formulation is sufficient. However, if the algorithm is to be operating for extended periods of time, it is desirable to have the more recent measurements weighted more heavily in the estimation. An exponential forgetting of old data can be implemented in a simple fashion by multiplying the old value of each summation by a forgetting factor prior to adding the current data. For example, to compute the current value of the summation of the control signal, the (1,2) element of the M matrix:

$$M_{1,2}(k) = f\ M_{1,2}(k-1) + u_1(k)$$

The forgetting factor f is chosen by selection of a time constant τ_{ff}.

$$f = 1 - \frac{\Delta t}{\tau_{ff}}$$

where Δt is the control law sample period. Typical values used in this report are: $\Delta t = 0.0125$ seconds, $\tau_{ff} = 300 - 800$ seconds.

3.1.2 Estimation for Two Redundant Surfaces

Consider a model with two redundant control surfaces to be a paraboloid of the form:

$$J(u_1, u_2) = c_o + c_1 u_1 + c_2 u_2 + c_3 u_1^2 + c_4 u_1 u_2 + c_5 u_2^2$$

The inclusion of the $c_4 u_1 u_2$ term is not obvious, since the aerodynamic model used in this study does not contain any direct drag due to the product of u_1 and u_2. It can be expected that this term will be non-zero in actual flight, so it is included in the development of the algorithm.

Following the same steps as the method for one control surface:

$$\begin{bmatrix} J_1 \\ J_2 \\ J_3 \\ . \\ . \\ . \end{bmatrix} = \begin{bmatrix} 1 & u_{1_1} & u_{2_1} & u_{1_1}^2 & u_{1_1}u_{2_1} & u_{2_1}^2 \\ 1 & u_{1_2} & u_{2_2} & u_{1_2}^2 & u_{1_2}u_{2_2} & u_{2_2}^2 \\ 1 & u_{1_3} & u_{2_3} & u_{1_3}^2 & u_{1_3}u_{2_3} & u_{2_3}^2 \\ . & . & . & . & . & . \\ . & . & . & . & . & . \\ . & . & . & . & . & . \end{bmatrix} \begin{bmatrix} c_o \\ c_1 \\ c_2 \\ c_3 \\ c_4 \\ c_5 \end{bmatrix}$$

$$\begin{bmatrix} \sum 1 & \sum u_1 & \sum u_2 & \sum u_1^2 & \sum u_1u_2 & \sum u_2^2 \\ \sum u_1 & \sum u_1^2 & \sum u_1u_2 & \sum u_1^3 & \sum u_1^2u_2 & \sum u_1u_2^2 \\ \sum u_2 & \sum u_1u_2 & \sum u_2^2 & \sum u_1^2u_2 & \sum u_1u_2^2 & \sum u_2^3 \\ \sum u_1^2 & \sum u_1^3 & \sum u_1^2u_2 & \sum u_1^4 & \sum u_1^3u_2 & \sum u_1^2u_2^2 \\ \sum u_1u_2 & \sum u_1^2u_2 & \sum u_1u_2^2 & \sum u_1^3u_2 & \sum u_1^2u_2^2 & \sum u_1u_2^3 \\ \sum u_2^2 & \sum u_1u_2^2 & \sum u_2^3 & \sum u_1^2u_2^2 & \sum u_1u_2^3 & \sum u_2^4 \end{bmatrix} \begin{bmatrix} c_o \\ c_1 \\ c_2 \\ c_3 \\ c_4 \\ c_5 \end{bmatrix} = \begin{bmatrix} \sum J \\ \sum u_1J \\ \sum u_2J \\ \sum u_1^2J \\ \sum u_1u_2J \\ \sum u_2^2J \end{bmatrix}$$

This equation is solved using a linear equation solver. It is not practical, or desirable, to solve this using explicit inversion of the 6-by-6 matrix. For this study, the solution was found by calling a LINPACK algorithm for symmetric linear equation solutions.

To help ensure good numerical properties of the linear equation solution, a scaling of the units should be considered. The condition number of the above matrix can be large if the signals u_1 and u_2 are measured in radians, for instance. To achieve a lower condition number, the units of degrees were chosen for this study, which is a reasonable normalization of the signal magnitudes.

The computational aspects of this method for higher numbers of redundant control surfaces may be a limiting factor if the on-board computational resources are limited.

3.2 Optimization

The least squares estimator is allowed to observe the response of the aircraft to the excitation signal for a period of time before any attempt is made to compute the optimal surface positions.

To compute the optimal surface positions, the least squares model is explicitly differentiated to solve for the extremal value of the redundant controls. For one redundant surface, the optimum position is found from:

$$J = c_o + c_1u_1 + c_2u_1^2 \tag{3.1}$$

$$\frac{\partial J}{\partial u_1} = c_1 + 2c_2 u_{1_{opt}} = 0 \tag{3.2}$$

$$u_{1_{opt}} = \frac{-c_1}{2c_2} \tag{3.3}$$

For two redundant surfaces, the optimum position is found from:

$$J = c_o + c_1 u_1 + c_2 u_2 + c_3 u_1^2 + c_4 u_1 u_2 + c_5 u_2^2 \tag{3.4}$$

$$\frac{\partial J}{\partial u_1} = c_1 + 2c_3 u_{1_{opt}} + c_4 u_{2_{opt}} = 0 \tag{3.5}$$

$$\frac{\partial J}{\partial u_2} = c_2 + c_4 u_{1_{opt}} + 2c_5 u_{2_{opt}} = 0 \tag{3.6}$$

$$\begin{bmatrix} -c_1 \\ -c_2 \end{bmatrix} = \begin{bmatrix} 2c_3 & c_4 \\ c_4 & 2c_5 \end{bmatrix} \begin{bmatrix} u_{1_{opt}} \\ u_{2_{opt}} \end{bmatrix} \tag{3.7}$$

$$\begin{bmatrix} u_{1_{opt}} \\ u_{2_{opt}} \end{bmatrix} = -\begin{bmatrix} 2c_3 & c_4 \\ c_4 & 2c_5 \end{bmatrix}^{-1} \begin{bmatrix} c_1 \\ c_2 \end{bmatrix} \tag{3.8}$$

$$= \frac{-1}{4c_3c_5 - c_4^2} \begin{bmatrix} 2c_5 & -c_4 \\ -c_4 & 2c_3 \end{bmatrix} \begin{bmatrix} c_1 \\ c_2 \end{bmatrix} \tag{3.9}$$

$$= \frac{1}{c_4^2 - 4c_3c_5} \begin{bmatrix} 2c_1c_5 - c_2c_4 \\ -c_1c_4 + 2c_2c_3 \end{bmatrix} \tag{3.10}$$

The optimal signals output from this optimization method may be discontinuous when the system is disturbed by wind gusts and sensor noise. This is especially true when the estimation has not had enough time to gather a sufficient amount of data, the disturbance environment is severe, or if the excitation signals are too small. Under extremely poor conditions, it is possible for the least squares paraboloid to be very flat and the extremal value of the model to be far from the current position. For these reasons, the optimal signals are passed through signal limiters and filtered. Second-order low pass filters were chosen to provide a smooth response in the optimal command when the optimization is first turned on. The low pass filters used in this study are:

$$\frac{a^2}{(s+a)^2} \qquad a = 0.04 \text{ rad/sec}$$

3.3 Optimization During Climb

The objective for optimization during climb is to optimize the rate of climb for a fixed throttle setting while tracking a commanded calibrated airspeed or Mach number. However, the sensing of climb rate is very susceptible to disturbance from wind gusts and sensor noise. It is reasonable to expect the measured energy rate to be disturbed less by wind gusts, so it is selected as the objective for optimization.

There is a significant complication to simply optimizing $\dot{E}_{meas}$ in that this quantity is changing due to performance variations as the Mach and altitude change. In fact, these performance variations will dwarf the small drag changes due to movement of the redundant control surfaces. To allow the variations due to the redundant surface deflections to be optimized, the altitude effects will be removed by using a model of the expected performance for a nominal aileron position. Without this correction, we can expect to be trying to find the maximum of a curve like shown in Figure 3.2.

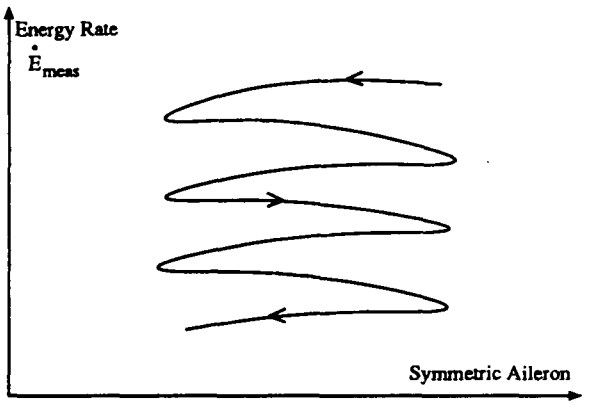

Figure 3.2: Complication With Optimization During Climb

The basic objective of the correction is to remove most of the drift in the observed energy rate to allow the adaptive controller to detect an optimum aileron position. So, the performance criteria in the optimization is:

$$J = \Delta\dot{E} = \dot{E}_{meas} - \dot{E}_{model}$$

A block diagram of the adaptive controller for optimization during climb is shown in Figure 3.3. The trim performance model is computed by an algorithm described by the flowchart in Figure 3.4. The quantities h_{cmd} and $\dot{h}_{cmd}$ are the altitude and altitude rate commands from the guidance system discussed in Section 4.2 on the climb trajectory guidance law. $\dot{E}_{meas}$ is the current measured total aircraft energy and is also described in Section 4.2. The performance model is computed by trimming out the stored aircraft model along the commanded path. Currently, this algorithm is implemented by calling the least squares aerodynamic database iteratively to achieve equilibrium. In practice, it will be much more practical to store a simplified trim model of the aerodynamics and engine performance on-board the aircraft. This model does not need (and should not include) the redundant surface effects – only the trim drag and thrust as functions of altitude, velocity and power setting, for nominal positions of the redundant surfaces, are required.

It is important to stress that the performance of the adaptive controller is not sensitive to the accuracy of the aerodynamic model used. The primary need for the model is to remove some of the drift of energy rate during the climb. If the model is inaccurate it will have little bearing on the performance of the adaptive controller.

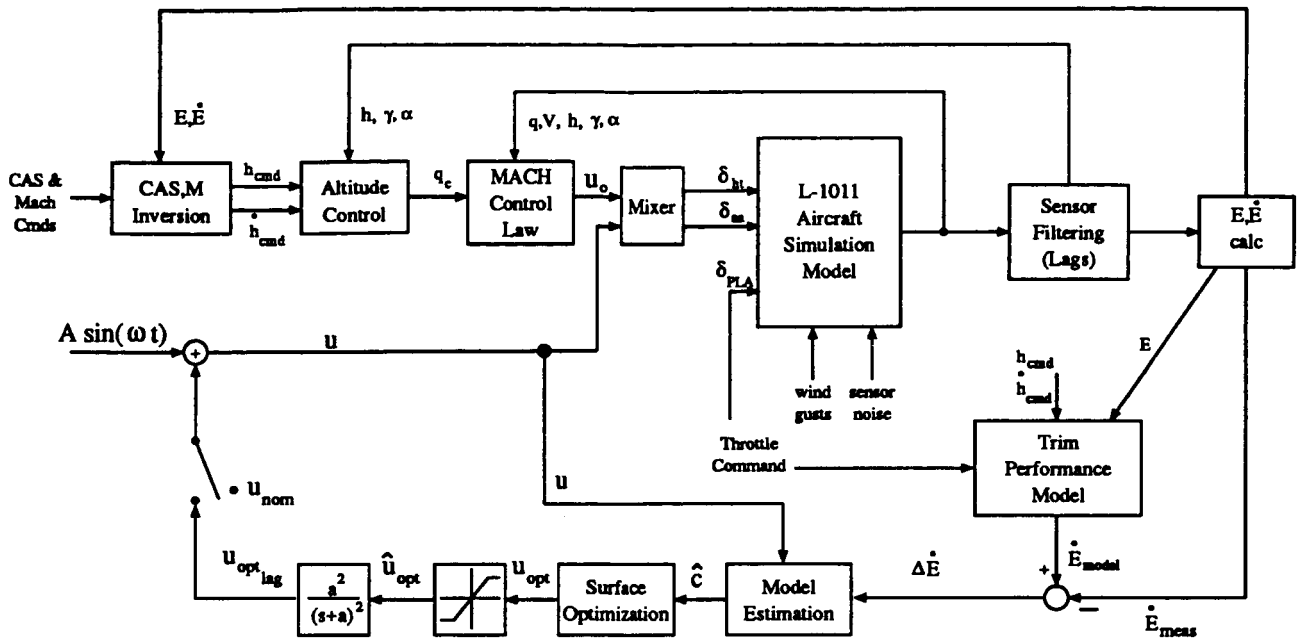

Figure 3.3: Block Diagram of Optimization During Climb Adaptive Controller

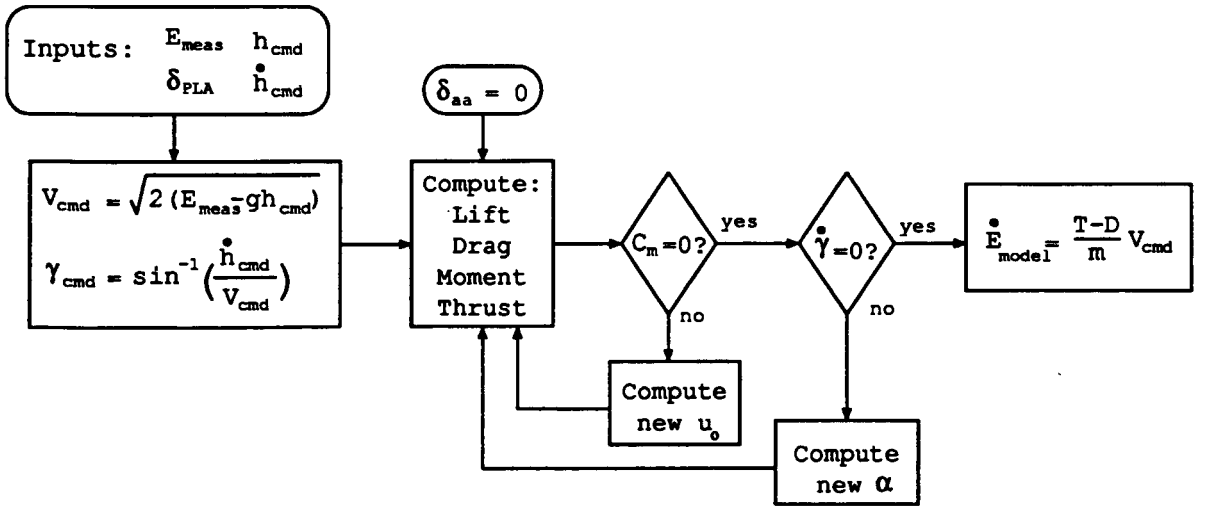

Figure 3.4: Flowchart of Trim Performance Computation

3.4 Control Effector Mixing

The control surfaces are run through a mixer to help decouple the adaptive control system responses, in a feedforward fashion, from the aircraft guidance and control laws. The excitation commands to the redundant surfaces (u_1 and u_2) will disturb the pitch axis of the aircraft and produce inner-loop autopilot responses. Also, the optimal drag configuration may be a function of the vehicle angle of attack and tail surface positions, so a feedforward command from the inner loop control signal (u_o) to the redundant surfaces (δ_{aa} and δ_{fl}) may help decouple the response due to environmental disturbances. Both of these types of cross coupling effects can be minimized with a feedforward mixing of the surfaces to provide the controllers with effective surfaces that will provide decoupled control.

Consider a mixer as shown in Figure 3.5.

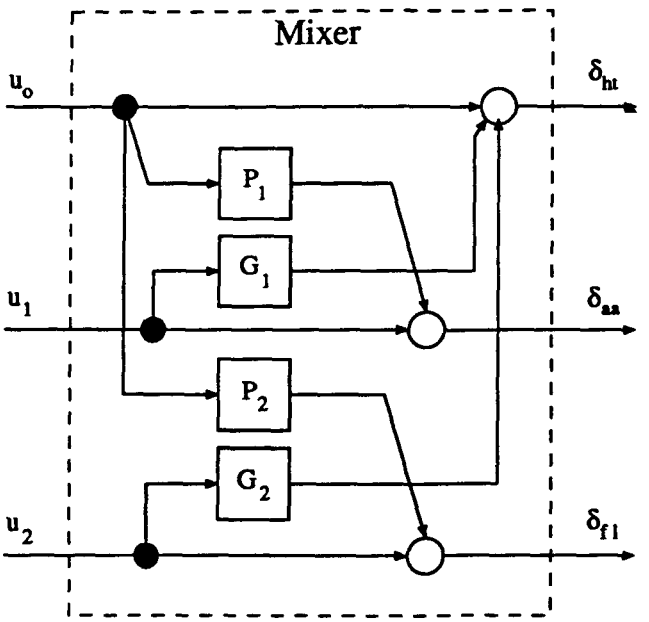

Figure 3.5: Control Effector Mixing to Reduce Cross-Coupling

This mixer can be written in matrix form:

$$\begin{bmatrix} \delta_{ht} \\ \delta_{aa} \\ \delta_{fl} \end{bmatrix} = \begin{bmatrix} 1 & G_1 & G_2 \\ P_1 & 1 & 0 \\ P_2 & 0 & 1 \end{bmatrix} \begin{bmatrix} u_o \\ u_1 \\ u_2 \end{bmatrix}$$

The gains G_1 and G_2 provide a feedforward path to the inner loop control system to compensate for the pitching moments and lift caused by deflections of the redundant surfaces. These gains command the correct amount of pitch control effector to provide a net zero moment for no change to the lift coefficient. This implicitly requires a change in the vehicle angle of attack.

Consider the least squares model for lift and moment.

$$C_L = C_{L_o} + C_{L_\alpha}\alpha + C_{L_{ht}}\delta_{ht} + C_{L_{aa}}\delta_{aa} + C_{L_{fl}}\delta_{fl} + C_{L_q}\frac{q\bar{c}}{2V_t} \tag{3.11}$$

$$C_M = C_{M_o} + C_{M_\alpha}\alpha + C_{M_{ht}}\delta_{ht} + C_{M_{aa}}\delta_{aa} + C_{M_{fl}}\delta_{fl} + C_{M_q}\frac{q\bar{c}}{2V_t} \tag{3.12}$$

For a specified lift coefficient $C_{L_{spec}}$ and $C_M = 0$, and considering δ_{fl} to be fixed at its current value, this can be solved for δ_{ht} in terms of δ_{aa}:

$$\begin{bmatrix} C_{L_{ht}} & C_{L_{aa}} \\ C_{M_{ht}} & C_{M_{aa}} \end{bmatrix} \begin{bmatrix} \delta_{ht} \\ \delta_{aa} \end{bmatrix} = \begin{bmatrix} C_{L_{spec}} - C_{L_o} - C_{L_\alpha}\alpha - C_{L_{fl}}\delta_{fl} \\ -C_{M_o} - C_{M_\alpha}\alpha - C_{M_{fl}}\delta_{fl} \end{bmatrix}$$

For the purposes of this derivation, everything in the above equation can be considered constant except δ_{ht}, δ_{aa} and α. To solve for δ_{ht} in terms of δ_{aa}, differentiate with respect to α:

$$\begin{bmatrix} C_{L_{ht}} & C_{L_{aa}} \\ C_{M_{ht}} & C_{M_{aa}} \end{bmatrix} \begin{bmatrix} \frac{\partial\delta_{ht}}{\partial\alpha} \\ \frac{\partial\delta_{aa}}{\partial\alpha} \end{bmatrix} = \begin{bmatrix} -C_{L_\alpha} \\ -C_{M_\alpha} \end{bmatrix}$$

$$\begin{bmatrix} \frac{\partial\delta_{ht}}{\partial\alpha} \\ \frac{\partial\delta_{aa}}{\partial\alpha} \end{bmatrix} = \frac{1}{C_{L_{ht}}C_{M_{aa}} - C_{L_{aa}}C_{M_{ht}}} \begin{bmatrix} C_{M_{aa}} & -C_{L_{aa}} \\ -C_{M_{ht}} & C_{L_{ht}} \end{bmatrix} \begin{bmatrix} -C_{L_\alpha} \\ -C_{M_\alpha} \end{bmatrix}$$

$$\begin{bmatrix} \frac{\partial\delta_{ht}}{\partial\alpha} \\ \frac{\partial\delta_{aa}}{\partial\alpha} \end{bmatrix} = \frac{1}{C_{L_{ht}}C_{M_{aa}} - C_{L_{aa}}C_{M_{ht}}} \begin{bmatrix} -C_{M_{aa}}C_{L_\alpha} + C_{L_{aa}}C_{M_\alpha} \\ C_{M_{ht}}C_{L_\alpha} - C_{L_{ht}}C_{M_\alpha} \end{bmatrix}$$

$$G_1 \equiv \frac{\partial\delta_{ht}}{\partial\delta_{aa}} = \frac{\frac{\partial\delta_{ht}}{\partial\alpha}}{\frac{\partial\delta_{aa}}{\partial\alpha}} = \frac{-C_{M_{aa}}C_{L_\alpha} + C_{L_{aa}}C_{M_\alpha}}{C_{M_{ht}}C_{L_\alpha} - C_{L_{ht}}C_{M_\alpha}}$$

Similarly, δ_{ht} in terms of δ_{fl}, holding δ_{aa} constant,

$$G_2 = \frac{\partial\delta_{ht}}{\partial\delta_{fl}} = \frac{-C_{M_{fl}}C_{L_\alpha} + C_{L_{fl}}C_{M_\alpha}}{C_{M_{ht}}C_{L_\alpha} - C_{L_{ht}}C_{M_\alpha}}$$

The gains P_1 and P_2 are intended to deflect the active aileron and outboard flap to stay on the predicted line of minimum drag when the horizontal tail is deflected to reject environmental disturbances.

Expressions for P_1 and P_2 will be derived later, during the derivation of the analytical optimization in Appendix B, but it is not clear that it makes sense to implement the control in this fashion in a production aircraft. This would put the active ailerons and outboard flaps in the inner loop feedback path, which may impact the certifiability of the primary control system. The simulations shown in this report use the value of zero for P_1 and P_2.

3.5 Sensor Filtering

The sensors used for the adaptive control and the outer loop guidance controllers are filtered to reduce the effects of random disturbances. A full implementation of the adaptive controller would likely get its sensor information from an inertial system that provides the functionality of this filtering, and more.

The following table shows the sensors that are filtered in the simulation and the break frequency of the filters. All of the filters are first order lag filters.

Sensor	Bandwidth (rad/sec)
V_t	5
h	2
γ	5
α	10
$\dot{V}_t$	10

3.6 Excitation Signal Considerations

The adaptive controller requires that enough information be present in the sensor signals to be able to form a model of the system. This is accomplished with the injection of sinusoidal signals to the redundant surfaces. The larger the amplitude of the excitation signal, the more information the adaptive controller has, and the better it will perform. As the disturbance environment becomes more severe, it is expected that the amplitude of the excitation signal must increase for successful location of the optimum surface positions.

However, it is desirable to not use too large of an excitation signal, since large deviations of the redundant surfaces from their optimum positions will carry a corresponding penalty in drag and autopilot performance. If the adaptive algorithm will only operate for a short period of time, this may be acceptable. But if the adaptive algorithm will operate continuously over a long period of time, then the selection of an excitation signal amplitude requires a trade-off between accurately finding the optimum surface positions and encountering increased drag due to the surface deflections.

A Monte Carlo simulation analysis has been performed to analyze the relationships between excitation signal amplitude, excitation signal frequency, disturbance environment, and the performance of the adaptive controller. See Section 5.4 for this analysis.

Perhaps the best way to implement the adaptive controller in a production aircraft is to have the adaption occur periodically during the flight, as the flight condition changes merit it. This allows the use of large excitation signal amplitudes to accurately find the optimum

surface positions, while not incurring the penalty associated with large surface deflections for long periods of time.

It would even be practical to develop a database of knowledge about an aircraft's optimum surface positions as a function of flight condition. This would allow the freedom to turn off the adaption on a gusty day, and just command the stored values of optimum surface positions. The database can be maintained on smooth days, or smooth potions of the flight, to account for the aging of the vehicle.

3.6.1 Excitation of Multiple Effectors

Each redundant surface is excited by a sinusoidal signal of a different frequency. It is important to ensure that the information provided to the adaptive controller is sufficient, and the relationship between the multiple excitation signal frequencies can play an important role. A plot of the independent variables should trace out a good coverage of the independent variable space, but it should also do so in a relatively short period of time. For this study, a ratio of frequencies of 3:2 was chosen for the two excitation signals.

Chapter 4

Guidance and Control Laws

Guidance and control laws have been designed and implemented for the purpose of this study, and are described here to document the simulation analysis of the adaptive controller. The adaptive controller does not depend on these particular guidance and control laws, although it does assume that these or similar G&C laws are in place.

The particular guidance and control laws used in this study have a more general form than typical production systems for transport-sized aircraft, but are very useful in the G&C development and simulation environment due to their highly parameterized formulation. The guidance and control laws use aircraft model data (aerodynamic and propulsive) directly, so development of G&C laws and closed loop simulations for new aircraft applications requires little effort.

4.1 Altitude and Velocity Hold Guidance Law

The altitude and velocity hold guidance law is used for maintaining a constant altitude and airspeed during cruise. The inputs are the commanded altitude and velocity, h_{cmd} and V_{cmd}, and the necessary feedback signals, h, V_t, and γ. The feedback signals are the measured and filtered quantities described earlier. See Figure 4.1 for a block diagram of this guidance law.

A desired altitude rate is formed by:

$$\dot{h}_{des} = b_h(h_{cmd} - h)$$

where b_h is a bandwidth gain of 0.13 rad/sec. This is converted to a flight path angle

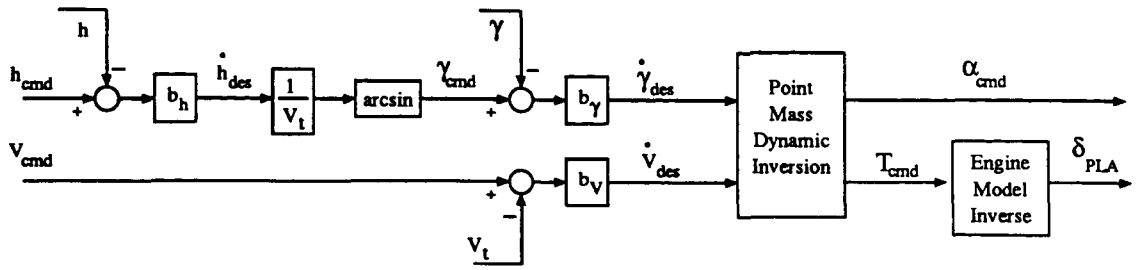

Figure 4.1: Block Diagram of Altitude and Velocity Hold Guidance Law

command based on the current airspeed.

$$\gamma_{cmd} = sin^{-1}\left(\frac{\dot{h}_{des}}{V_t}\right)$$

The flight path angle and velocity loops are described by:

$$\dot{\gamma}_{des} = b_\gamma(\gamma_{cmd} - \gamma)$$

$$\dot{V}_{des} = b_V(V_{cmd} - V)$$

The solution of the angle-of-attack and throttle setting that achieves $\dot{\gamma}_{des}$ and $\dot{V}_{des}$ is implemented by an inversion of the point mass equations of motion, including the least squares aerodynamic model. Consider the point mass equations of motion:

$$\dot{V}_t = -\frac{D}{m} - g\sin\gamma + T\cos\alpha \tag{4.1}$$

$$\dot{\gamma} = \frac{L}{mV_t} - \frac{g\cos\gamma}{V_t} + \frac{T\sin\alpha}{mV_t} \tag{4.2}$$

The above equations can be solved for a commanded thrust and angle-of-attack, T_{cmd} and α_{cmd}, to achieve the desired rates of change, $\dot{V}_{des}$ and $\dot{\gamma}_{des}$.

$$\dot{V}_{des} = -\frac{D(\alpha_{cmd})}{m} - g\sin\gamma + T_{cmd}\cos\alpha_{cmd} \tag{4.3}$$

$$\dot{\gamma}_{des} = \frac{L(\alpha_{cmd})}{mV_t} - \frac{g\cos\gamma}{V_t} + \frac{T_{cmd}\sin\alpha_{cmd}}{mV_t} \tag{4.4}$$

An iterative scheme is used to solve for the commands that satisfy the above equations. The aerodynamic model used during this inversion is the least squares approximate model.

The computed angle-of-attack command is passed on to an attitude controller, and the thrust command is passed directly to the throttle command by inverting the engine model.

4.2 Climb Trajectory Guidance Law

The climb trajectory guidance law, shown in Figure 4.2, is used during climbing flight to track a specified calibrated airspeed until a desired cruise Mach number is reached. Once the cruise Mach is achieved, the climb continues tracking this Mach number. The throttle is fixed at a climb throttle setting.

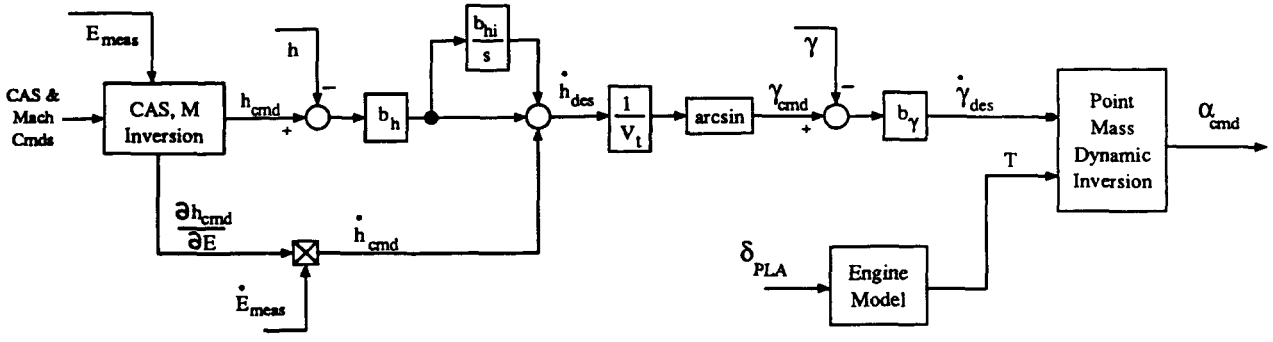

Figure 4.2: Block Diagram of Climb Trajectory Guidance Law

The essence of this guidance law is that the pitch moment effectors must be used to track the desired speed, since we are not free to change the throttle setting during the climb.

The method used in this report to control V_{CAS} and M is to compute an altitude command that will achieve the desired airspeed through a trade-off between kinetic and potential energy. This altitude command will be used as an input to an altitude controller.

This method of computing the altitude command is not unique. The approach taken here is to assume that a maneuver to the commanded altitude happens over a relatively short period of time, so that the total energy of the aircraft doesn't change. See Figure 4.3.

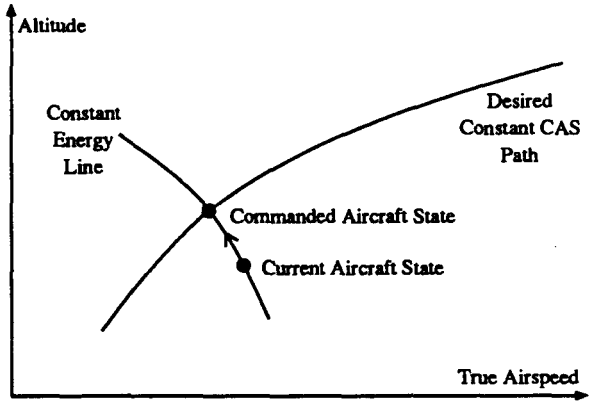

Figure 4.3: Calibrated Airspeed Tracking Strategy

The altitude command is found by inverting a model of the calibrated airspeed, or Mach number, as a function of altitude for the current measured energy level. For example,

consider a model of the calibrated airspeed:

$$V_{CAS} = F(E_{meas}, h) = \left\{ 5a_{sl}^2 \left(\left[\frac{p(h)}{p_{sl}} \left(\left[\frac{V_t^2}{5a(h)^2} + 1 \right]^{\frac{7}{2}} - 1 \right) + 1 \right]^{\frac{2}{7}} - 1 \right) \right\}^{\frac{1}{2}} \quad (4.5)$$

where,

$$E_{meas} = gh + \frac{1}{2}V_t^2 \quad (4.6)$$

$$V_t = \sqrt{2(E_{meas} - gh)} \quad (4.7)$$

$$a(h) = \text{speed of sound} \quad (4.8)$$

$$p(h) = \text{ambient air pressure} \quad (4.9)$$

The inverse of the calibrated airspeed model can be represented by:

$$h_{cmd} = F^{-1}(E_{meas}, V_{CAS_{cmd}})$$

It is also desirable to provide the altitude controller with a feedforward altitude rate command. To achieve this, the partial derivative of the altitude command with respect to the energy level is found. This is then multiplied by the measured energy rate:

$$\frac{\partial h_{cmd}}{\partial E} = \left[F^{-1}(E_{meas} + \Delta E, V_{CAS_{cmd}}) - F^{-1}(E_{meas}, V_{CAS_{cmd}}) \right] \frac{1}{\Delta E} \quad (4.10)$$

$$\dot{E}_{meas} = g\dot{h} + V_t\dot{V}_t \quad (4.11)$$

$$= gV_t \sin\gamma + V_t\dot{V}_t \quad (4.12)$$

$$\dot{h}_{cmd} = \frac{d\, h_{cmd}}{d\, t} = \frac{\partial h_{cmd}}{\partial E}\dot{E}_{meas} \quad (4.13)$$

where the quantities $V_t, \gamma,$ and$\dot{V}_t$ are measured and filtered.

The altitude tracking is similar to the altitude and velocity hold controller, with the exception that the throttle is fixed and there is an integral term added to the altitude error:

$$\dot{h}_{des} = b_h \left(1 + \frac{b_{hi}}{s} \right) (h_{cmd} - h) + \dot{h}_{cmd}$$

where b_h is a bandwidth gain of 0.13 rad/sec, and b_{hi} is an integrator bandwidth gain of 0.04 rad/sec.

$$\gamma_{cmd} = sin^{-1} \left(\frac{\dot{h}_{des}}{V_t} \right)$$

$$\dot{\gamma}_{des} = b_\gamma(\gamma_{cmd} - \gamma)$$

The dynamic inversion does not include the velocity rate equation, since the throttle is fixed and the velocity is not being explicitly controlled.

$$\dot{\gamma} = \frac{L}{mV_t} - \frac{g\cos\gamma}{V_t} + \frac{T\sin\alpha}{mV_t} \tag{4.14}$$

The above equation can be solved for a commanded angle-of-attack, α_{cmd}, to achieve $\dot{\gamma}_{des}$.

$$\dot{\gamma}_{des} = \frac{L(\alpha_{cmd})}{mV_t} - \frac{g\cos\gamma}{V_t} + \frac{T\sin\alpha_{cmd}}{mV_t} \tag{4.15}$$

The thrust T used in the above solution is found by evaluating the engine model at the current altitude and throttle setting.

The computed angle-of-attack command is passed on to an attitude controller.

4.3 Pitch Attitude Controller

The pitch attitude is controlled by a simple dynamic inversion controller that commands a pitch rate q_{cmd} to track the desired angle-of-attack α_{cmd}. See Figure 4.4.

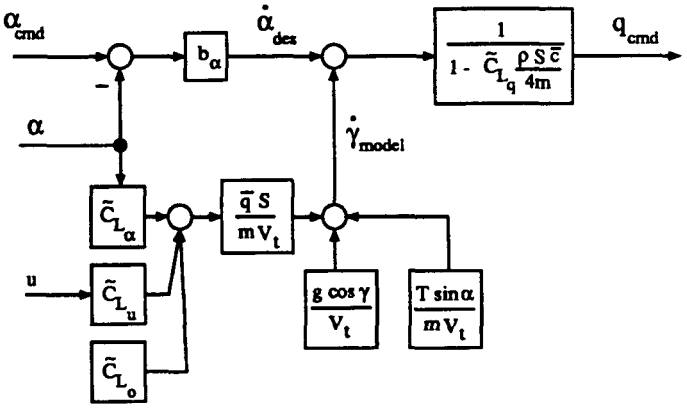

Figure 4.4: Pitch Attitude Controller

$$\dot{\alpha}_{des} = b_\alpha(\alpha_{cmd} - \alpha)$$

The pitch dynamics are inverted to achieve the desired $\dot{\alpha}$.

$$\dot{\alpha} = q - \dot{\gamma} \tag{4.16}$$

$$\dot{\gamma} = \frac{L}{mV_t} - \frac{g\cos\gamma}{V_t} + \frac{T\sin\alpha}{mV_t} \tag{4.17}$$

$$q_{cmd} = \dot{\alpha}_{des} + \dot{\gamma}_q \tag{4.18}$$

$$\dot{\gamma}_q \equiv \dot{\gamma}\,|_{\dot{q}=0} \tag{4.19}$$

The lift expression in this equation is written in terms of the effective controls u_o, u_1 and u_2. Deriving the aerodynamic coefficients in terms of these controls:

$$\begin{bmatrix} C_{L_{u_o}} \\ C_{L_{u_1}} \\ C_{L_{u_2}} \end{bmatrix} = \begin{bmatrix} 1 & P_1 & P_2 \\ G_1 & 1 & 0 \\ G_2 & 0 & 1 \end{bmatrix} \begin{bmatrix} C_{L_{ht}} \\ C_{L_{aa}} \\ C_{L_{fl}} \end{bmatrix} \tag{4.20}$$

$$\begin{bmatrix} C_{M_{u_o}} \\ C_{M_{u_1}} \\ C_{M_{u_2}} \end{bmatrix} = \begin{bmatrix} 1 & P_1 & P_2 \\ G_1 & 1 & 0 \\ G_2 & 0 & 1 \end{bmatrix} \begin{bmatrix} C_{M_{ht}} \\ C_{M_{aa}} \\ C_{M_{fl}} \end{bmatrix} \tag{4.21}$$

$$q_{cmd} = \dot{\alpha}_{des} + \frac{\bar{q}S}{mV_t}\left[C_{L_o} + C_{L_\alpha}\alpha + C_{L_{u_o}}u_o + C_{L_{u_1}}u_1 + C_{L_{u_2}}u_2 + C_{L_q}\frac{q\bar{c}}{2V_t}\right] \tag{4.22}$$

$$-\frac{g\cos\gamma}{V_t} + \frac{T_{cmd}\sin\alpha}{mV_t} \tag{4.23}$$

The feedback control deflection u_o that appears above is found by assuming that the moments will be trimmed.

$$C_M = C_{M_o} + C_{M_\alpha}\alpha + C_{M_{u_o}}u_o + C_{M_{u_1}}u_1 + C_{M_{u_2}}u_2 + C_{M_q}\frac{q\bar{c}}{2V_t} = 0 \tag{4.24}$$

$$\hat{u}_o = \frac{-1}{C_{M_{u_o}}}\left(C_{M_o} + C_{M_\alpha}\alpha + C_{M_{u_1}}u_1 + C_{M_{u_2}}u_2 + C_{M_q}\frac{q_{cmd}\bar{c}}{2V_t}\right) \tag{4.25}$$

$$\tag{4.26}$$

Substituting this in the equation for q_{cmd}:

$$q_{cmd} = \dot{\alpha}_{des} + \frac{\bar{q}S}{mV_t}\left[C_{L_o} + C_{L_\alpha}\alpha + C_{L_{u_1}}u_1 + C_{L_{u_2}}u_2 + C_{L_q}\frac{q_{cmd}\bar{c}}{2V_t}\right. \tag{4.27}$$

$$\left. -\frac{C_{L_{u_o}}}{C_{M_{u_o}}}\left(C_{M_o} + C_{M_\alpha}\alpha + C_{M_{u_1}}u_1 + C_{M_{u_2}}u_2 + C_{M_q}\frac{q_{cmd}\bar{c}}{2V_t}\right)\right] \tag{4.28}$$

$$-\frac{g\cos\gamma}{V_t} + \frac{T_{cmd}\sin\alpha}{mV_t} \tag{4.29}$$

Defining composite lift coefficients for zero moments:

$$\tilde{C}_{L_o} = C_{L_o} - C_{M_o}C_{L_{u_o}}/C_{M_{u_o}} \tag{4.30}$$

$$\tilde{C}_{L_{u_1}} = C_{L_{u_1}} - C_{M_{u_1}}C_{L_{u_o}}/C_{M_{u_o}} \tag{4.31}$$

$$\tilde{C}_{L_{u_2}} = C_{L_{u_2}} - C_{M_{u_2}}C_{L_{u_o}}/C_{M_{u_o}} \tag{4.32}$$

$$\tilde{C}_{L_\alpha} = C_{L_\alpha} - C_{M_\alpha}C_{L_{u_o}}/C_{M_{u_o}} \tag{4.33}$$

$$\tilde{C}_{L_q} = C_{L_q} - C_{M_q}C_{L_{u_o}}/C_{M_{u_o}} \tag{4.34}$$

$$\tag{4.35}$$

Rewriting q_{cmd} with these composite lift coefficients:

$$q_{cmd} = \dot{\alpha}_{des} + \frac{\bar{q}S}{mV_t}\left[\tilde{C}_{L_o} + \tilde{C}_{L_\alpha}\alpha + \tilde{C}_{L_{u_1}}u_1 + \tilde{C}_{L_{u_2}}u_2 + \tilde{C}_{L_q}\frac{q_{cmd}\bar{c}}{2V_t}\right] \tag{4.36}$$

$$-\frac{g\cos\gamma}{V_t} + \frac{T_{cmd}\sin\alpha}{mV_t} \tag{4.37}$$

Solving for q_{cmd}:

$$q_{cmd} = \frac{\dot{\alpha}_{des} + \frac{\bar{q}S}{mV_t}\left[\tilde{C}_{L_o} + \tilde{C}_{L_\alpha}\alpha + \tilde{C}_{L_{u_1}}u_1 + \tilde{C}_{L_{u_2}}u_2\right] - \frac{g\cos\gamma}{V_t} + \frac{T_{cmd}\sin\alpha}{mV_t}}{1 - \tilde{C}_{L_q}\frac{\rho S\bar{c}}{4m}} \tag{4.38}$$

4.4 Inner Loop Pitch Controller

The inner loop pitch controller computes the feedback command u_o to achieve the desired pitch rate. The controller used for this study is a general dynamic inversion controller for inner loop aircraft control called MACH (for Multi-Application Control). References [9], [10], [11], and [12] each contain a description of this control law.

Chapter 5

Simulation Analysis

The drag minimizing controllers described in this report were tested under a variety of operating conditions. This chapter presents simulations of the controllers and summary plots of a Monte Carlo simulation analysis.

This chapter is organized as follows:

1. Discussion of realism effects (wind gusts and sensor noise)
2. Simulations with no adaptive controller
3. Simulations of the basic adaptive controller
4. Monte Carlo simulation analysis of the basic adaptive controller
5. Simulations of optimization during climb
6. Simulations of optimization of multiple effectors

All of the level flight simulations are carried out at a commanded altitude of 37,000 feet, and a commanded airspeed of 803.5 feet/second (Mach 0.827).

The climb trajectory is specified by an initial condition at 10,000 feet and a calibrated airspeed of 320 knots (540 feet/second). The aircraft tracks a constant calibrated airspeed until it reaches a Mach number of 0.82, then it tracks this Mach number. The throttle is held fixed at a value of 46.5% of maximum thrust. At 10,000 feet, this amounts to a total thrust of about 51,000 pounds.

5.1 Realism Effects

The simulations presented were performed under three possible cases of realism effects:

1. No disturbances – to illustrate the algorithm operation
2. Light disturbances
3. Moderate disturbances

The Monte Carlo simulation analysis was performed with both light and moderate disturbance levels.

5.1.1 Dryden Wind Gust Model

The wind gust model was simulated as follows:

$$gust_{para} = \sigma\sqrt{\frac{2V}{L}}\left(\frac{1}{s+\frac{V}{L}}\right)\omega_n$$

$$gust_{perp} = \sigma\sqrt{\frac{V}{L}}\left(\frac{\sqrt{3}s+\frac{V}{L}}{s^2+\frac{2V}{L}s+\left(\frac{V}{L}\right)^2}\right)\omega_n$$

where: $\sigma = 1$ ft/sec for light wind gust levels, $\sigma = 5$ ft/sec for moderate wind gust levels, $\sigma = 10$ ft/sec for severe wind gust levels, $L = 1750$ feet, V = aircraft instantaneous velocity, and ω_n is white noise with zero mean and unit standard deviation. This model is consistent with the description of the Dryden gust model found on page 459 of the document ADDFL-TR-69-72, the guide for MIL-F-8785B. [6]

5.1.2 Sensor Noise Model

Sensor noise was simulated by passing zero mean white noise through low pass filters and adding these signals to the aircraft model's state variables. The standard deviations of the white noise are derived from the ARINC standards for Inertial Reference Systems, and are listed in the table below. [8]

	Standard Deviation
V	0.25 ft/sec
α	0.09 deg
q	0.1 deg/sec
γ	0.09 deg
h	5 $feet$
$\bar{q}$	1.0 lb/ft^2

To simulate light levels of sensor noise, the above 1σ values are divided by two.

5.2 Simulation With No Adaptive Controller

Figure A.1 shows the altitude hold and velocity controller simulated with no disturbance to show the transient due to imperfect trim of the guidance and control laws at the initial condition. This transient is present in all of the simulations, but may not be seen when it is drowned out by the random disturbances. The hang-off in airspeed and altitude from the commanded 803.5 feet/second and 37,000 feet is due to mismatches between the full aerodynamic model of the simulated aircraft and the simplified aerodynamic model used in the guidance laws and inner loop controller. The guidance laws do not include integral control, so the commands are not perfectly achieved at steady state.

Figures A.2 and A.3 show the altitude and velocity hold controller simulated with light and moderate disturbance levels to show the response of the nominal system for these disturbance levels.

5.3 Simulation of Basic Adaptive Controller

Simulations of the basic adaptive controller optimizing the active ailerons are shown in Figures A.4, A.5 and A.6.

Each simulation of the adaptive controller follows the sequence of events:

- 0 seconds: start excitation signal
- 0-50 seconds: allow initial condition transient to subside
- 50-200 seconds: estimation of model without optimization
- 200-end of simulation: optimization active

The simulations are run for 600 seconds for light disturbance levels, and for 800 seconds for moderate disturbance levels.

The excitation signal for these three simulations has an amplitude of 1.5 degrees and a frequency of 0.04 rad/sec.

For all three simulations, the initial position of the active ailerons is zero degrees, and the excitation signal initially oscillates the ailerons about this position until the adaptive controller is turned on.

Figure A.4 shows the operation of the adaptive controller with no disturbances. The optimal surface position is quickly and accurately located.

Figure A.5 and Figure A.6 show the adaptive controller simulated with light and moderate disturbance levels. The adaptive controller requires about 500 seconds to converge to the optimum surface position for light disturbances, and about 600-700 seconds for moderate disturbances.

5.4 Monte Carlo Simulation Analysis

Two series of simulation analyses were undertaken, one to evaluate the effect of changing the amplitude of the excitation signal and one to evaluate the effect of changing the frequency of the excitation signal. For both series of Monte Carlo simulations, 30 simulations were performed at each value of the independent variable, and the analysis was performed for both light and moderate levels of wind gusts and noise disturbance.

Each simulation follows the sequence of events described in Section 5.3, with one difference: the initial position of the active ailerons is at one degree, and the excitation signal is initially oscillating about this position until the adaptive controller is turned on.

There are two different ways of using the adaptive controller, and two corresponding criteria of evaluating how well the adaptive controller is working.

1. Run the adaption for a short period of time, then fly the aircraft with no adaption. The objective is to accurately locate the optimal surface positions.
2. Run the adaption continuously for a long period of time. The objective is to minimize the total fuel consumption, which is a trade-off between accurately finding the optimal surface positions and drag penalties due to large surface deflections.

The Monte Carlo simulation results are presented to evaluate the performance of the adaptive controller using both of the above criteria: final surface position and average thrust level.

The table below is a cross reference to the Monte Carlo simulation analysis summary plots. Each of the summary plots will show a solid line which is the average of all of the simulations performed at that value of the independent variable. The dashed lines represent plus and minus one standard deviation. The amplitude specified on the horizontal axis is the amplitude of the sine wave, or one half of the peak-to-peak magnitude of the excitation.

	Amplitude Sweep		Freq. Sweep
	Surface Position	Ave. Thrust	Surface Position
Light Dist.	Figure 5.1	Figure 5.2	Figure 5.3
Moderate Dist.	Figure 5.4	Figure 5.5	Figure 5.6

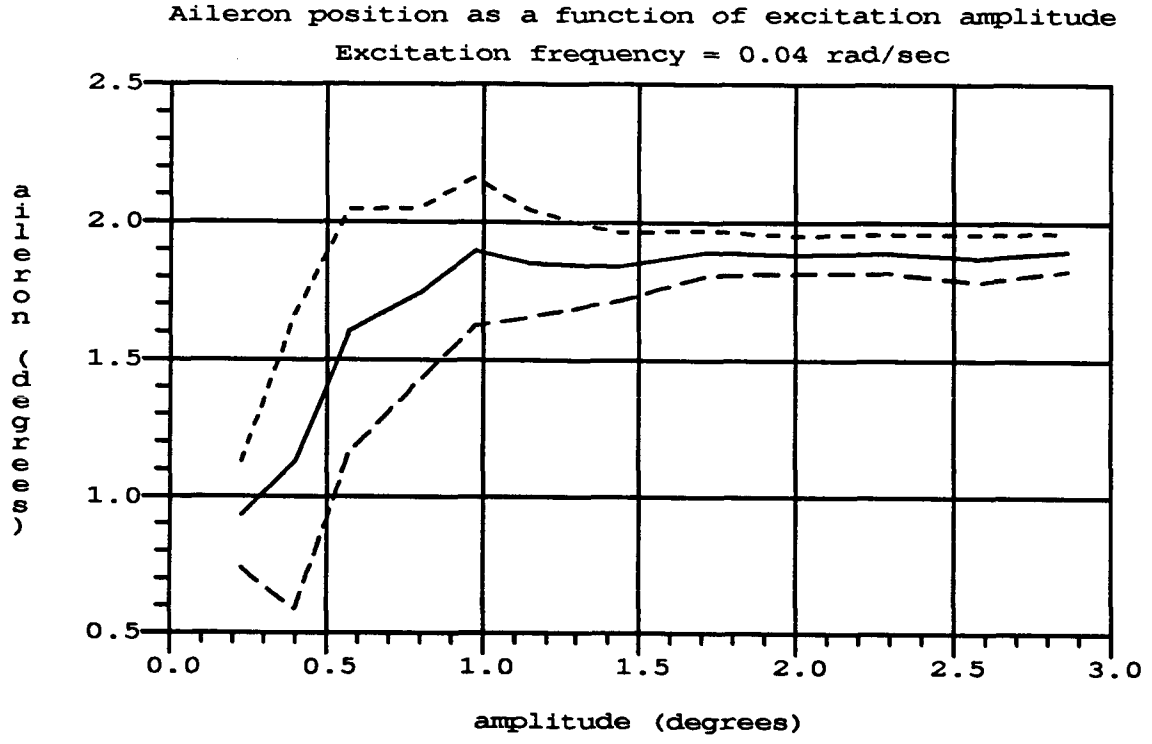

Figure 5.1: Amplitude Sweep, Final Optimum, Light Disturbance

As shown in Figures 5.1 and 5.4, the adaptive controller does not find the optimum surface position if the excitation amplitude is not large enough. For the light disturbance levels, the excitation signal needs to be above 0.7 degrees, and for moderate disturbance levels at least 1.3 degrees. As the excitation amplitude is increased above these values, the standard deviation of the result decreases, showing that the algorithm more reliably locates the optimum surface position with a stronger excitation. Above a certain amplitude of excitation, however, the algorithm is doing the best it can with the encountered disturbance environment, and the standard deviation stays flat. The optimal surface positions shown in these figures should be compared to the optimal values given in Section 2.5.

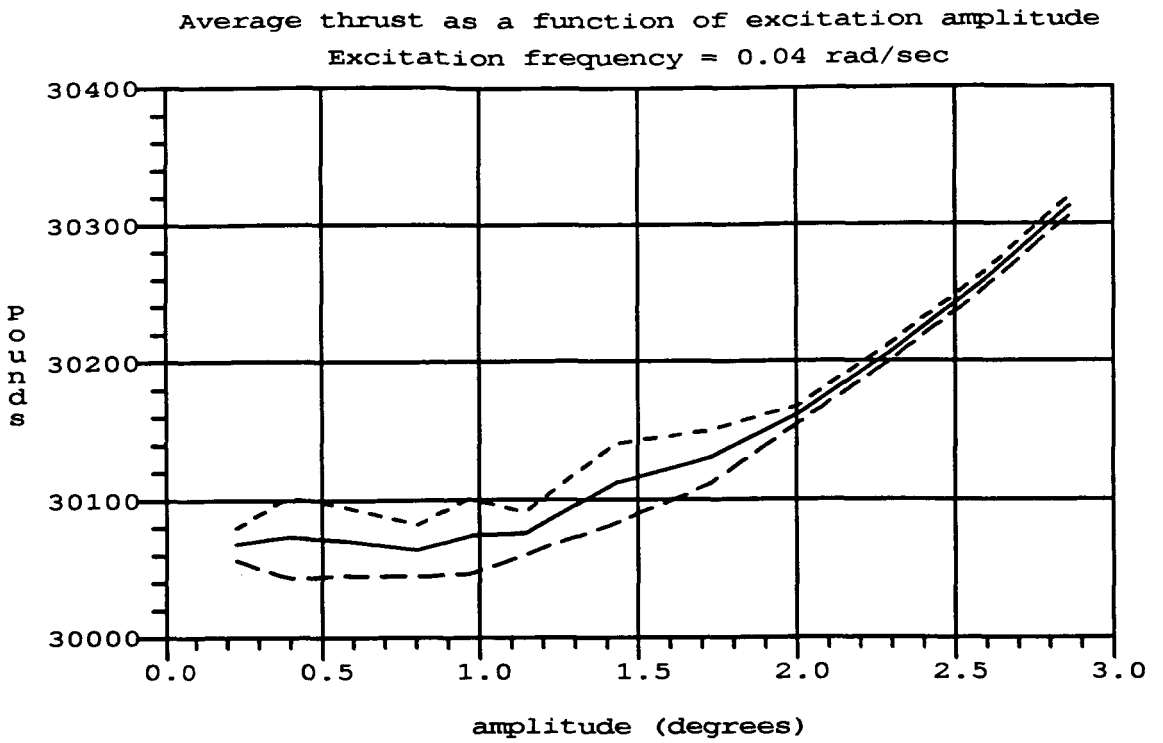

Figure 5.2: Amplitude Sweep, Average Thrust, Light Disturbance

Figures 5.2 and 5.5 show the variation of average thrust during the simulation with changes in the excitation amplitude. The results shown in these figures are tabulated from the same Monte Carlo simulation runs used in Figures 5.1 and 5.4. Since the active ailerons were started close to the minimum drag position for these simulations, these figures should be interpreted as showing the drag penalty of operating the adaptive controller continuously with a high amplitude excitation signal. As the amplitude increases, the surface spends too much time away from the optimal position, thus increasing the average thrust required.

Comparing Figure 5.1 with Figure 5.2, one can observe the trade-off between accurately locating the optimum surface position and the associated penalty in continuously operating the adaptive controller. To guarantee accurate detection of the optimum surface position, the excitation signal should be operated in the 1.5 to 2 degree range, but this carries an associated penalty of about 50 to 100 pounds of drag. Using the adaptive controller only until the optimum surface position is located, then shutting the adaption and the excitation signal off, achieves all of the benefits of the drag minimization without the corresponding penalty due to a large excitation signal. Similar conclusions can be made comparing Figure 5.1 with Figure 5.2.

Observing Figures 5.3 and 5.6, there does not seem to be a significant relationship between the frequency of excitation and the performance of the adaptive controller. There is some degradation of the adaptive controller performance at high frequencies of excitation in the range of the outer loop bandwidth, but this does not seem to be very significant.

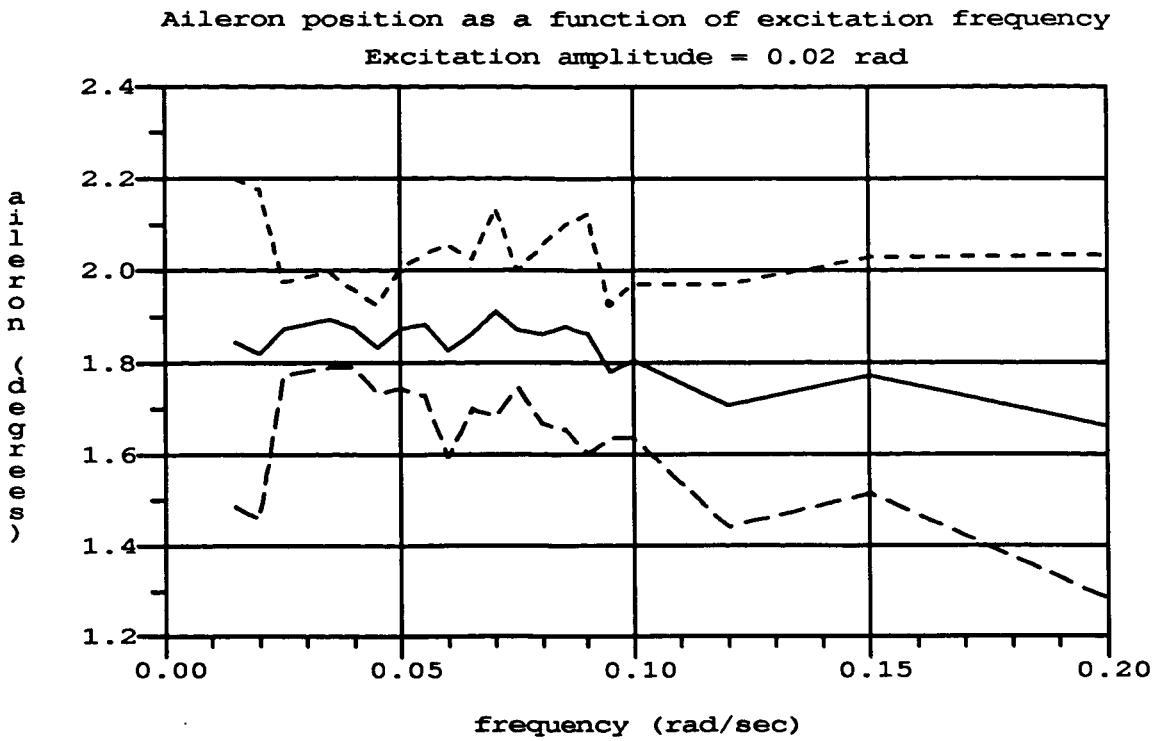

Figure 5.3: Frequency Sweep, Final Optimum, Light Disturbance

5.5 Simulation of Optimization During Climb

Figures A.7, A.8 and A.9 show simulations of the adaptive controller during climb for three levels of disturbance environment: none, light, and moderate, respectively. In all of these simulations, the initial position of the active ailerons is zero degrees. The forgetting time constant of the estimator is reduced to 500 seconds to allow the adaptive controller to track the optimal surface position as it changes.

The optimal surface position ($u_{1_{opt}}$) shown in these figures can be compared to the optimal surface positions given in Section 2.5, Table 2.3, shown as x's on the plot of the optimal surface position.

The plots of the optimal surface position ($u_{1_{opt}}$) show that the adaptive controller rapidly converges to a steady value slightly above the optimal value, and then tracks the optimal value as it changes slowly with time.

5.6 Simulation of Optimization of Multiple Effectors

Figures A.10, A.11 and A.12 show simulations of the adaptive controller applied to the simultaneous optimization of the active ailerons and outboard flaps for three levels of

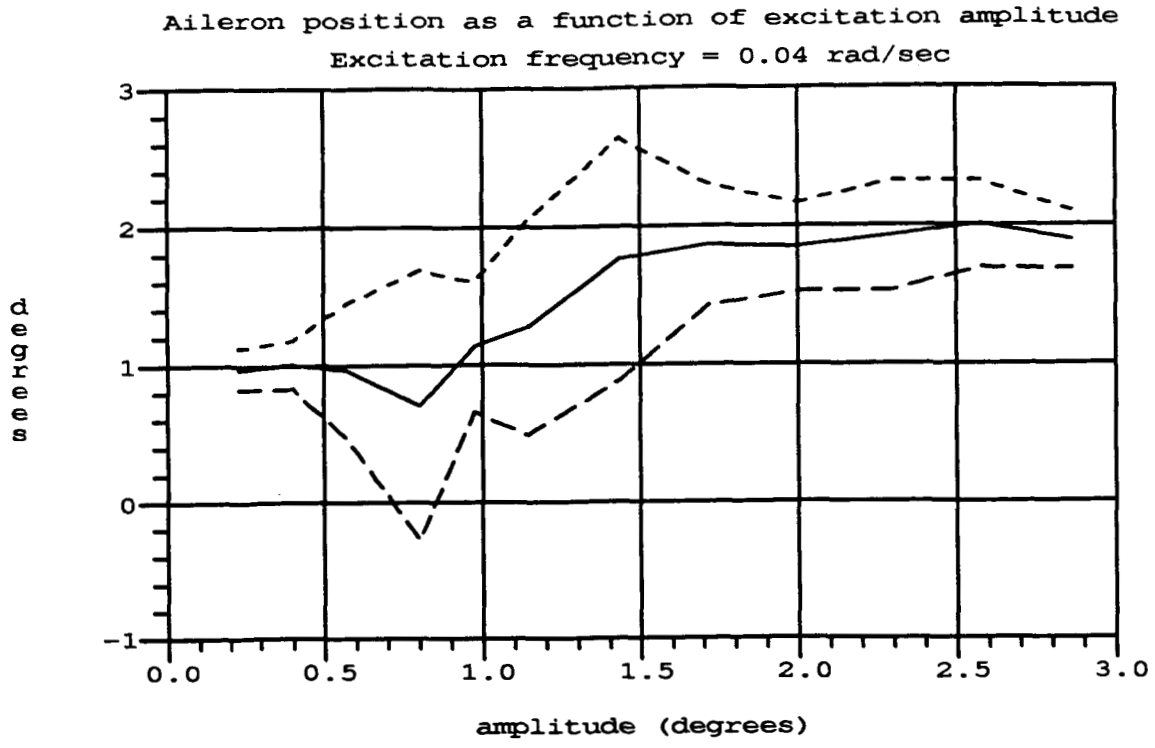

Figure 5.4: Amplitude Sweep, Final Optimum, Moderate Disturbance

disturbance environment: none, light, and moderate, respectively.

The plots of optimal active aileron and outboard flap positions ($u_{1_{opt}}$ and $u_{2_{opt}}$ respectively) as functions of time can be compared to the true optimal positions found in Section 2.5.

Observing Figure A.10, with no disturbances, the adaptive controller already has enough information to accurately compute the optimal surface positions when it is turned on at 400 seconds into the simulation.

Observing Figures A.11 and A.12, with light and moderate disturbances, the adaptive controller requires about 700 seconds to converge to the optimal surface positions.

The plots of the flap position versus the active aileron position are a graphical way of showing how well the two-dimensional space of independent variables is covered during the simulation.

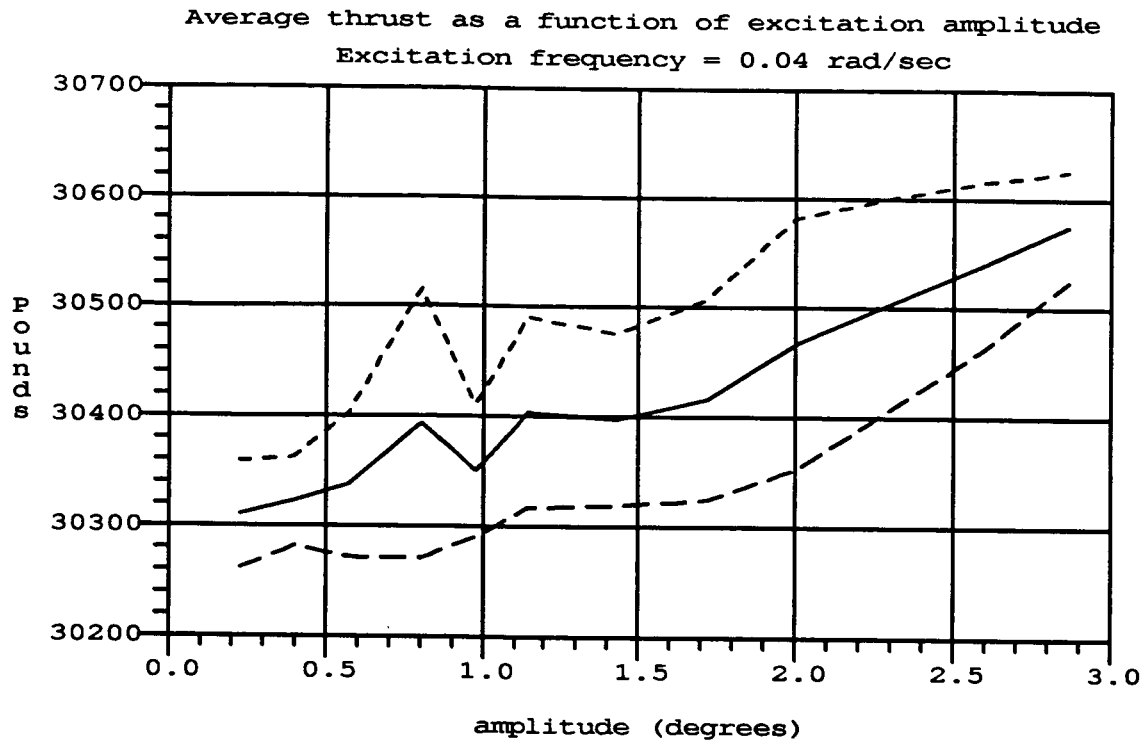

Figure 5.5: Amplitude Sweep, Average Thrust, Moderate Disturbance

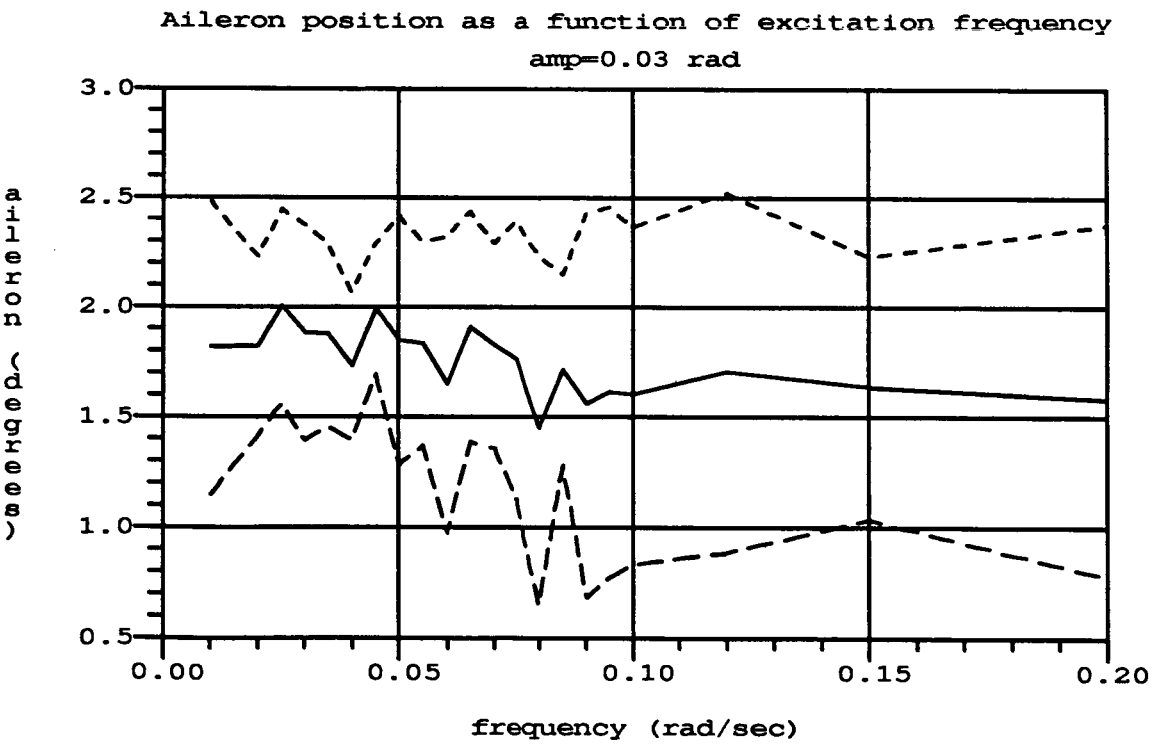

Figure 5.6: Frequency Sweep, Final Optimum, Moderate Disturbance

Chapter 6

Concluding Discussion

This report describes an adaptive controller used to minimize the drag of an aircraft by taking advantage of the available redundant control surfaces. The controller is based on the optimization of a performance model that is generated by least squares estimation. Sinusoidal excitation signals are applied to the redundant control surfaces to ensure that enough information is present in the observed sensor signals for the proper operation of the model estimation.

A Monte Carlo simulation analysis was performed under a realistic simulation environment that includes wind gusts, sensor noise, and differences between the simulated aircraft dynamics and the dynamics modeled in the controller. This analysis shows that for light disturbance environments the adaptive controller consistently and accurately locates the optimal active aileron position. For moderate disturbance environments, the adaptive controller requires more time to converge and the optimal solution contains discontinuities that require filtering.

The Monte Carlo simulation analysis investigated the influence of the excitation signal amplitude and frequency on the performance of the adaptive controller as measured by the computed optimal active aileron position and the average thrust level. The study shows that the adaptive controller more accurately locates the optimal surface position as the excitation signal amplitude is increased, as expected, and that the selection of the excitation signal frequency is not as critical. The analysis also quantified the corresponding drag penalty incurred when the adaptive controller is continuously operated for extended periods of time.

The adaptive control approach has been extended to operate during climbing flight, and several simulations show that this extension works. For light disturbance environments, the active aileron position converges to the optimum position, and continues to track the optimum position as it moves during the climb. This approach requires on-board storage of a special model of the basic aircraft aerodynamics and propulsion effects, however, the

convergence of the adaptive controller to the true optimal surface positions is not sensitive to the accuracy of this stored model,

The adaptive control method has also been extended to simultaneously optimize the active ailerons and the outboard flaps, and several simulations show that the adaptive controller performs well.

The benefits to be gained by minimization of aircraft drag are immense. A reduction in fuel consumption of 1% translates into a savings of about $100,000 annually for a typical commercial transport. For the aircraft model used in this report, accurate optimization of the active ailerons saves about 260 pounds of drag out of 30,000 pounds (0.87%), and simultaneous optimization of the outboard flaps and the active ailerons saves about 480 pounds of drag (1.6%). However, the significant result of this report is the demonstration of an adaptive control approach which can find the minimum drag configuration of an aircraft despite model mismatch, wind gusts, and sensor noise.

Appendix A

Simulation Time Histories

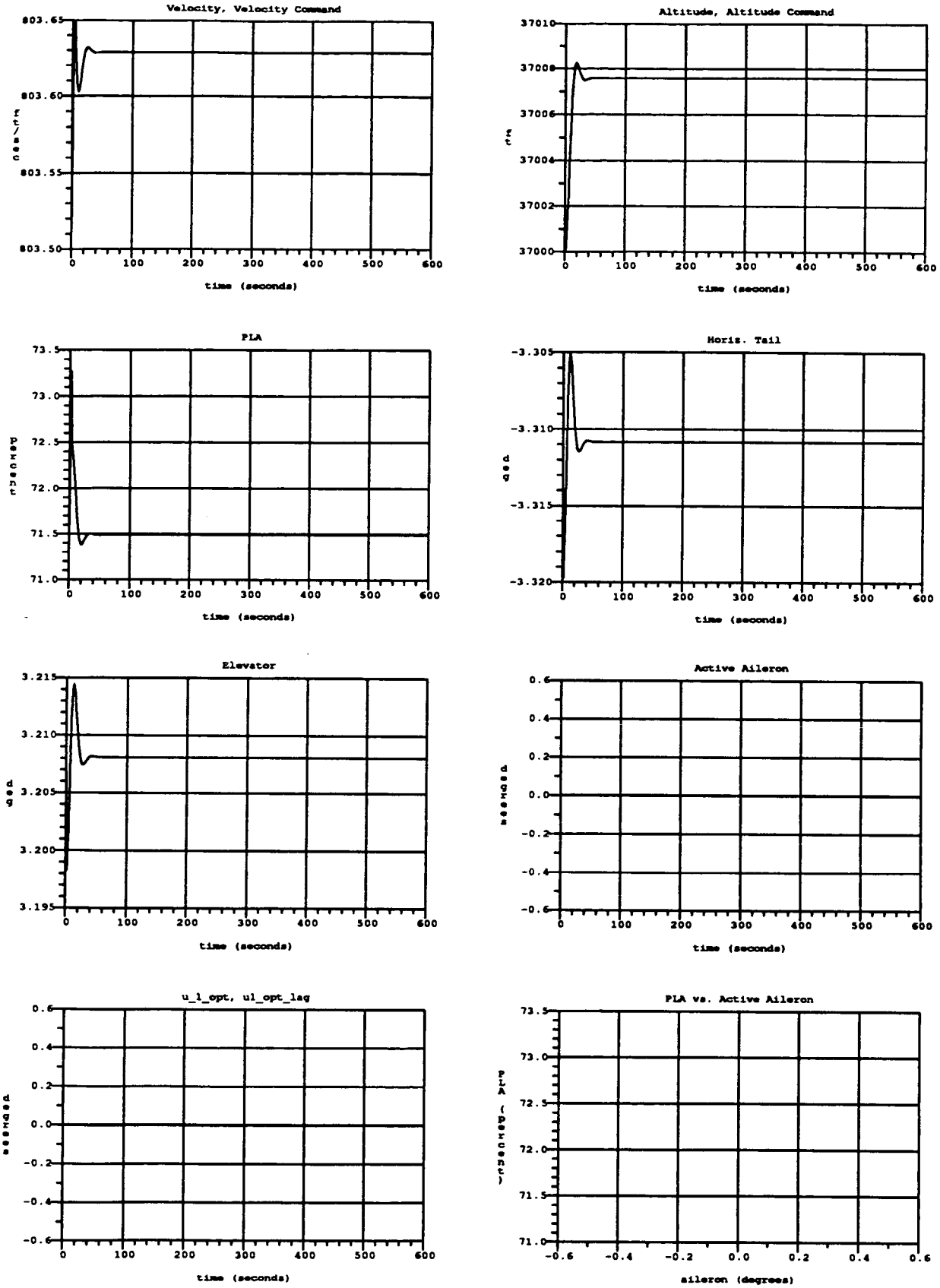

Figure A.1: Simulation With No Adaption, No Disturbance

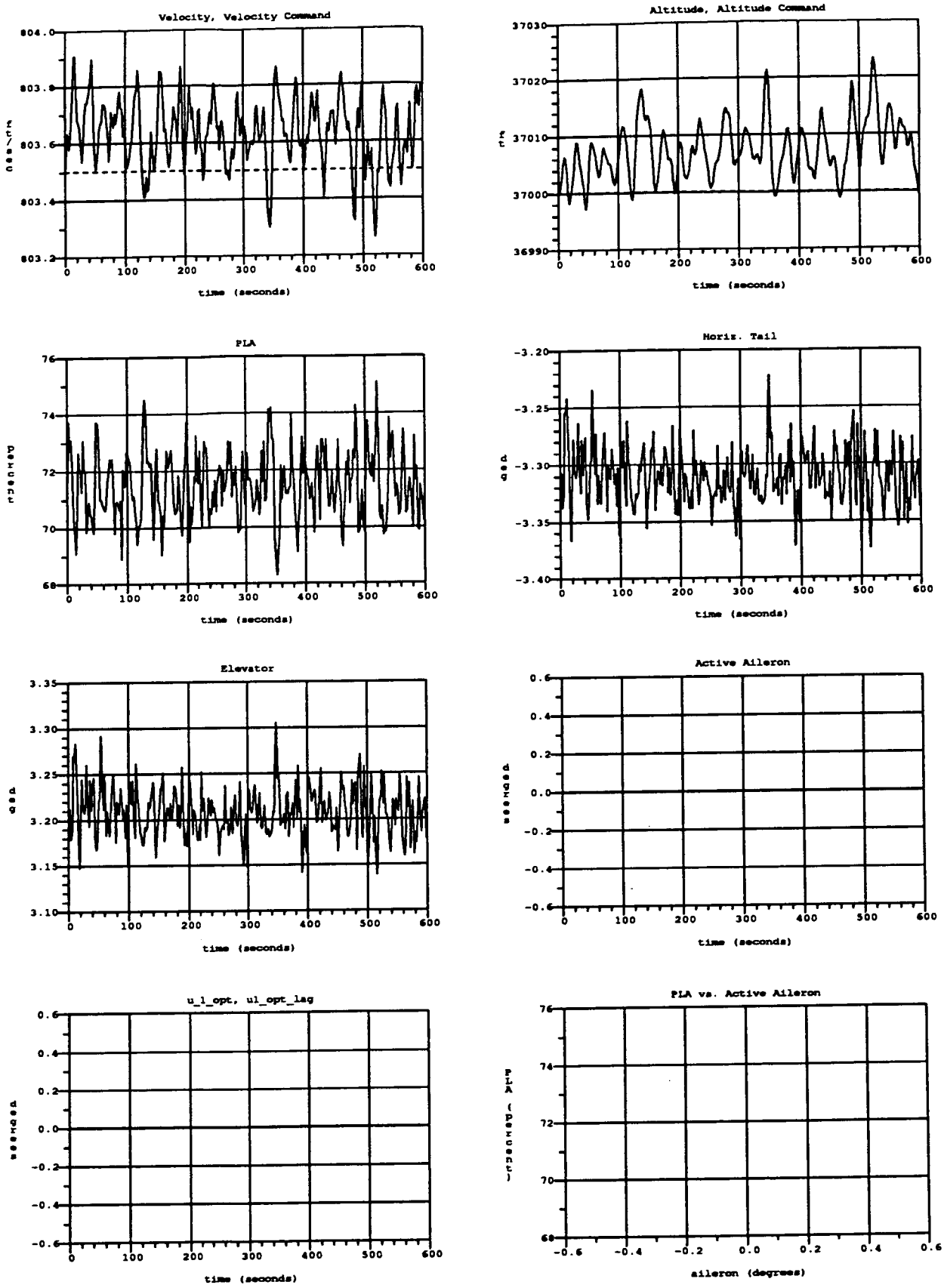

Figure A.2: Simulation With No Adaption, Light Disturbances

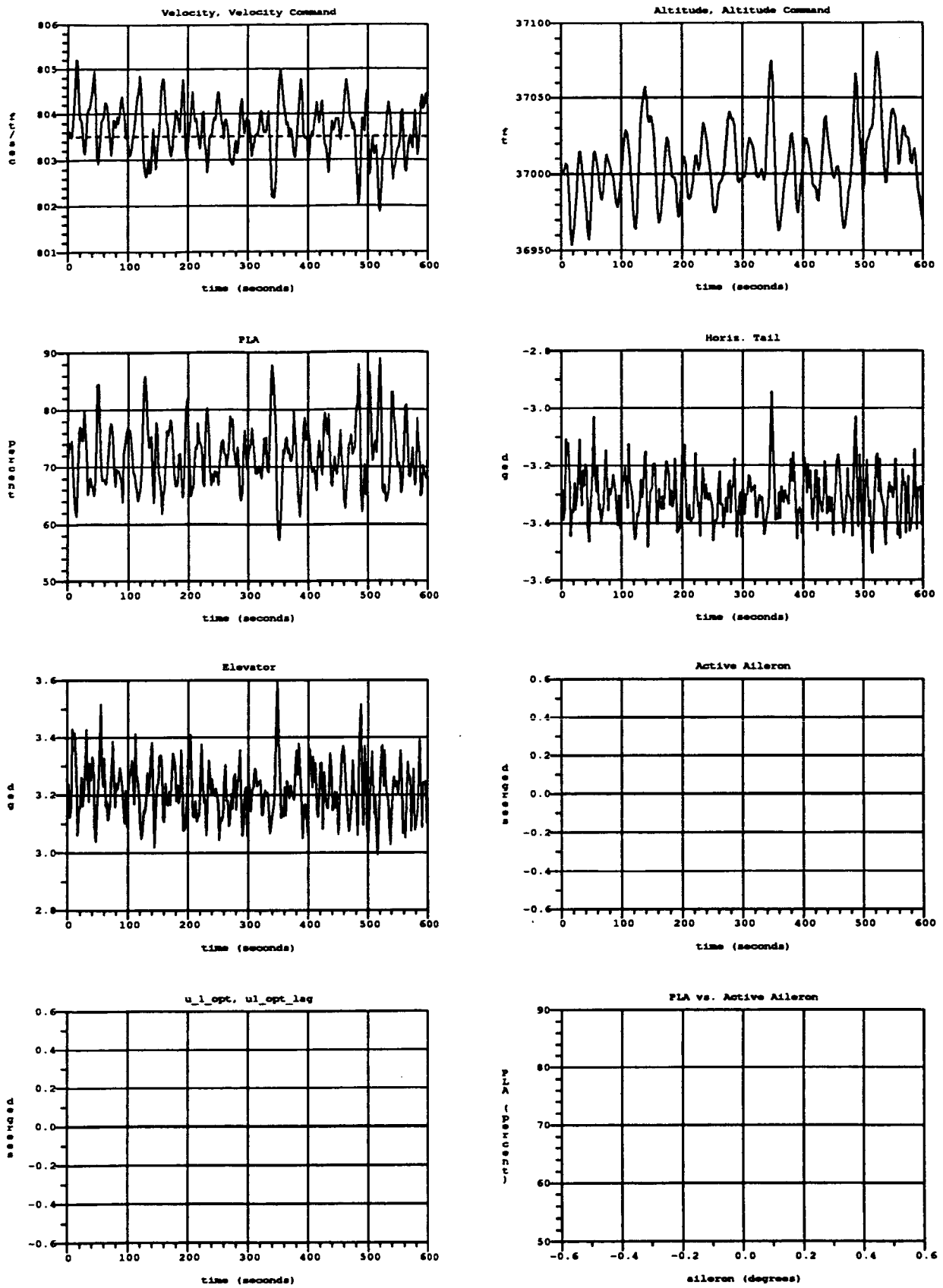

Figure A.3: Simulation With No Adaption, Moderate Disturbances

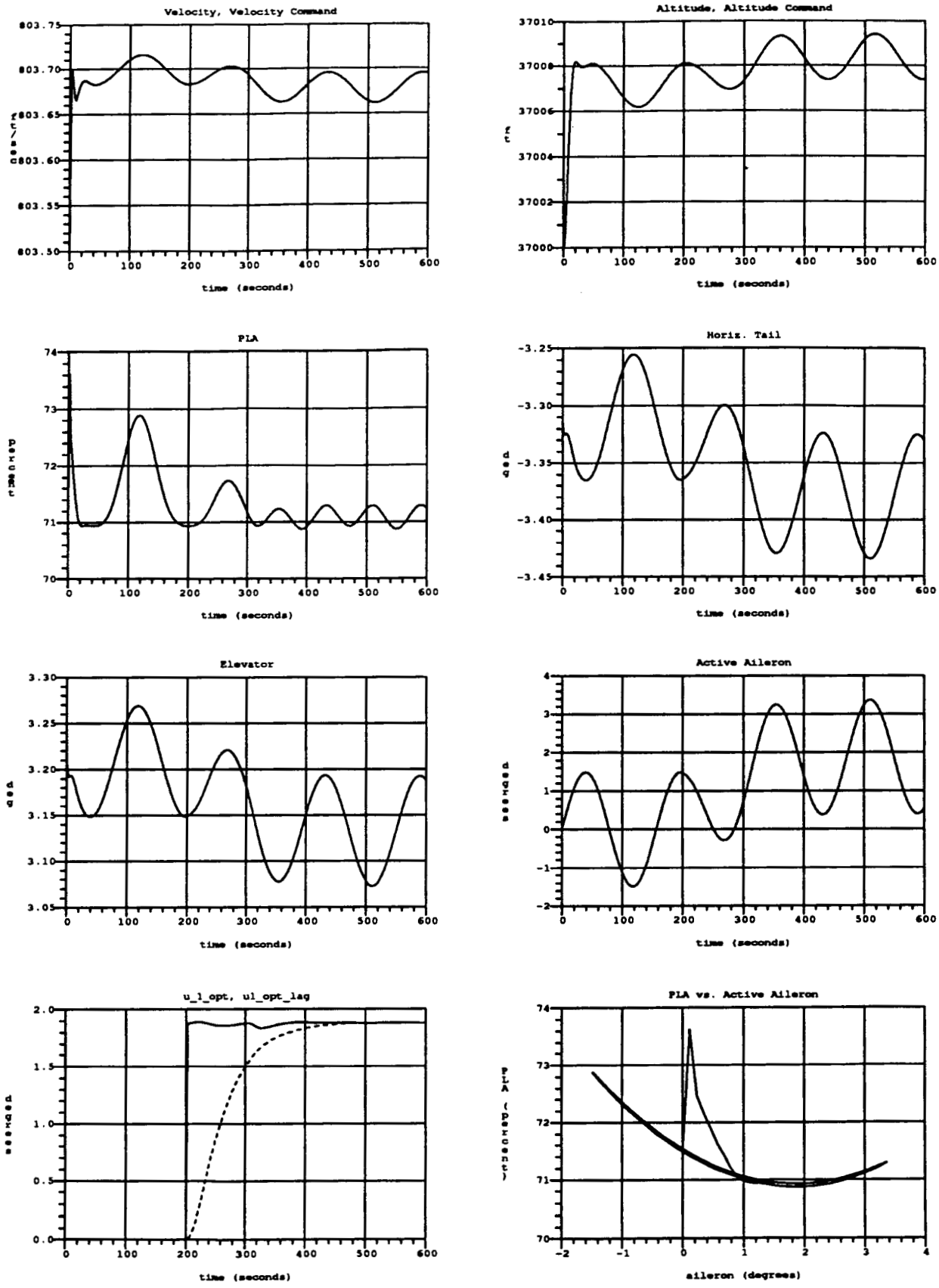

Figure A.4: Simulation of Basic Adaptive Controller, No Disturbance

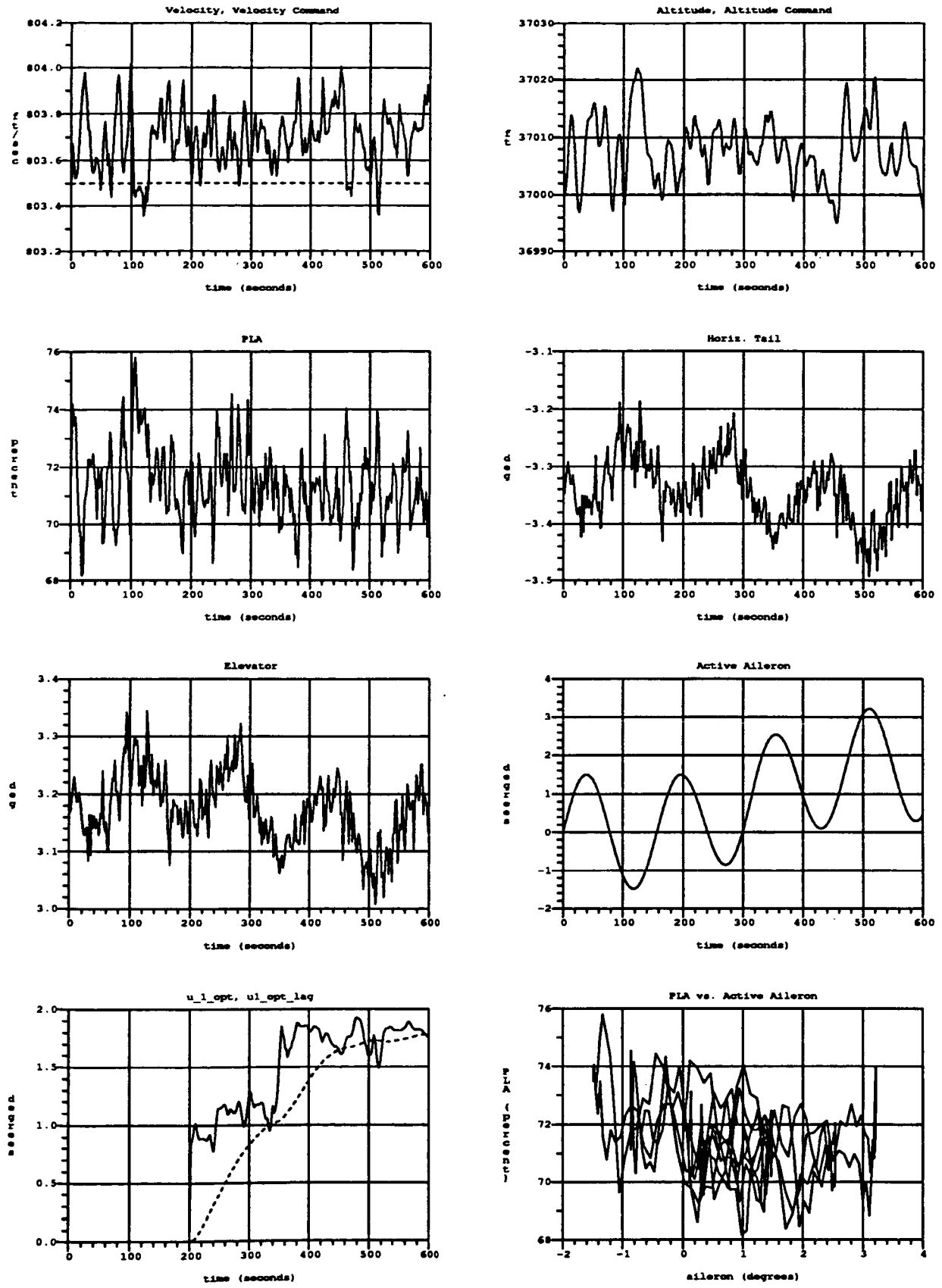

Figure A.5: Simulation of Basic Adaptive Controller, Light Disturbances

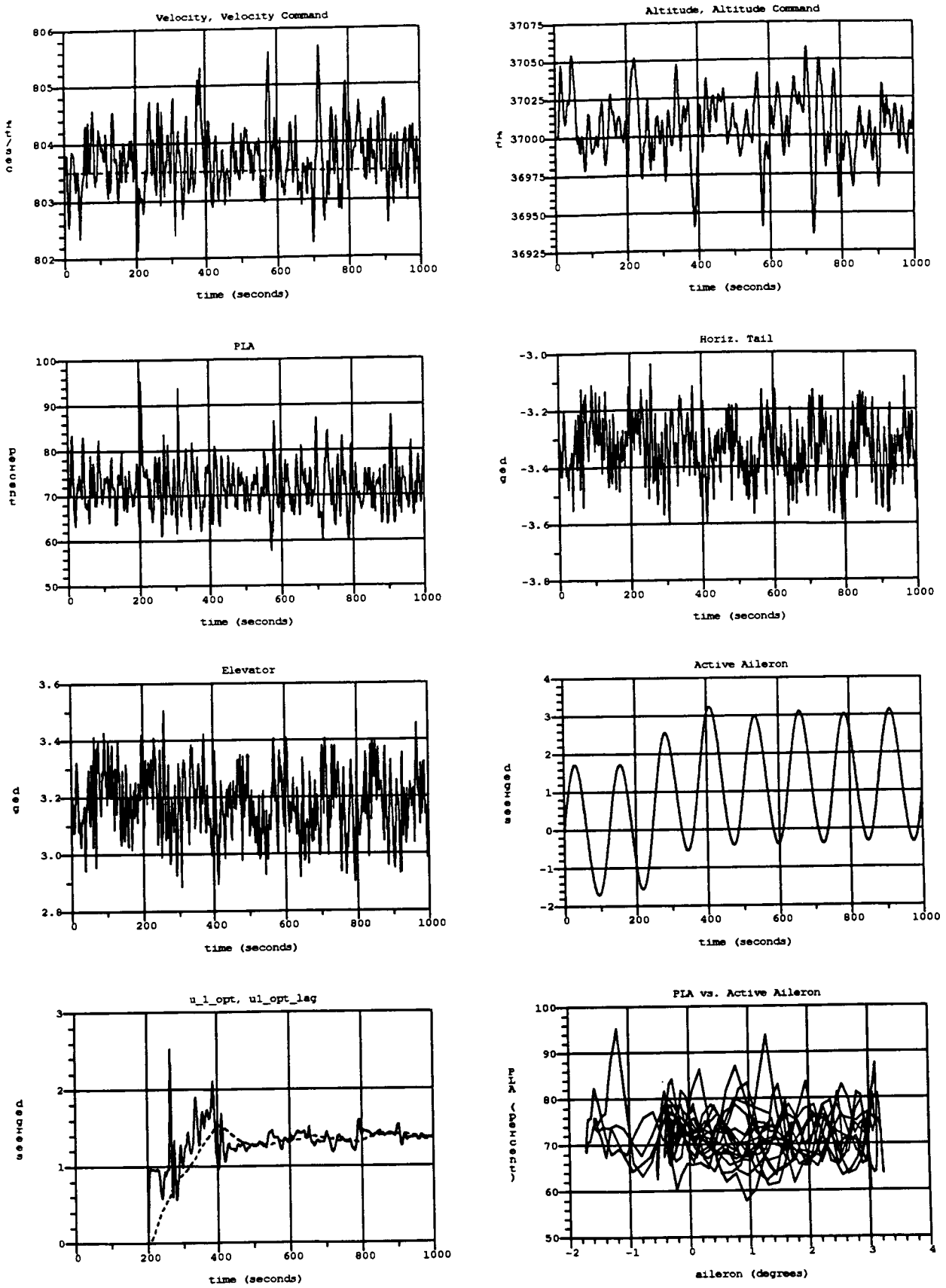

Figure A.6: Simulation of Basic Adaptive Controller, Moderate Disturbances

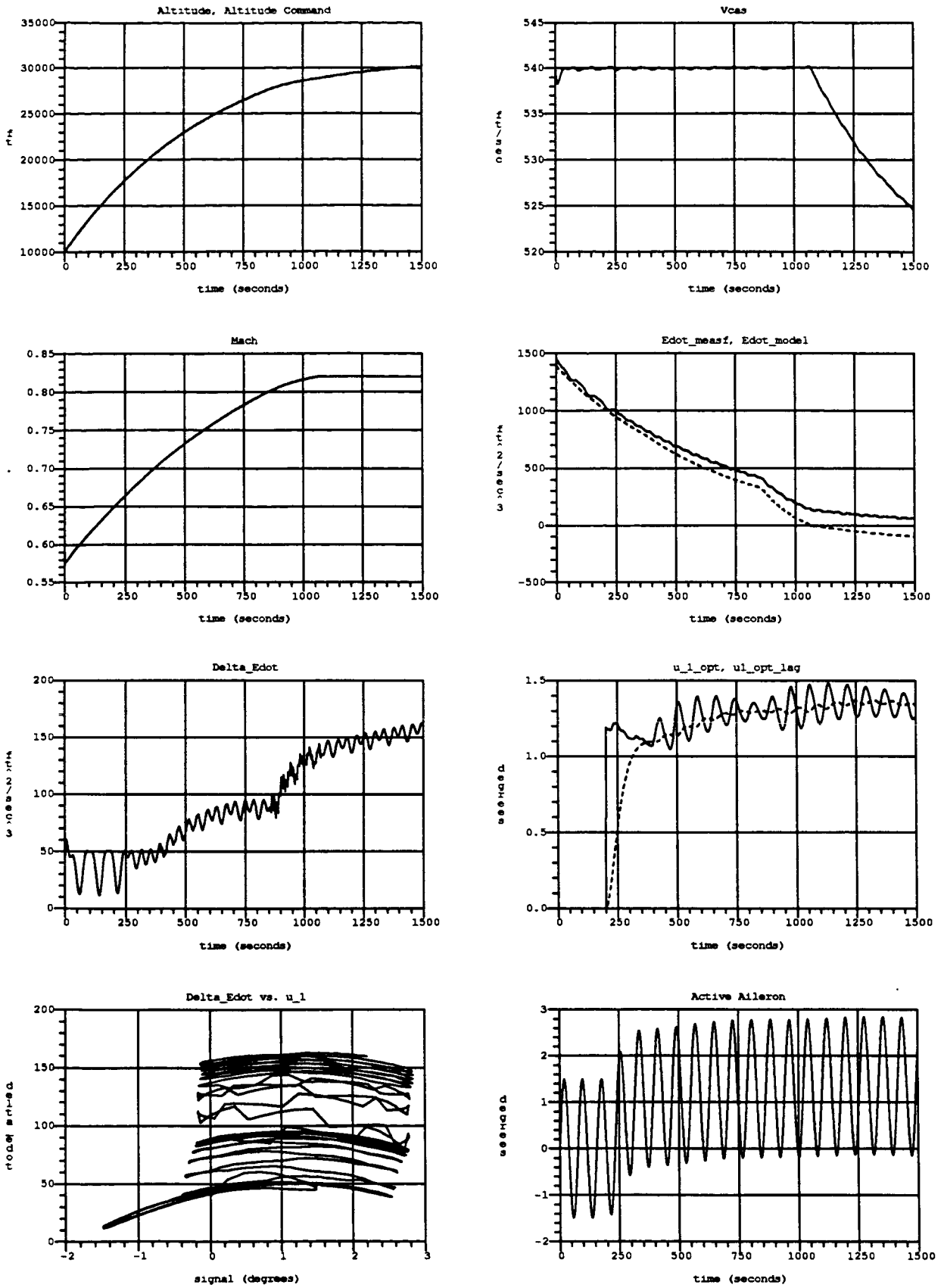

Figure A.7: Optimization During Climb, No Disturbance

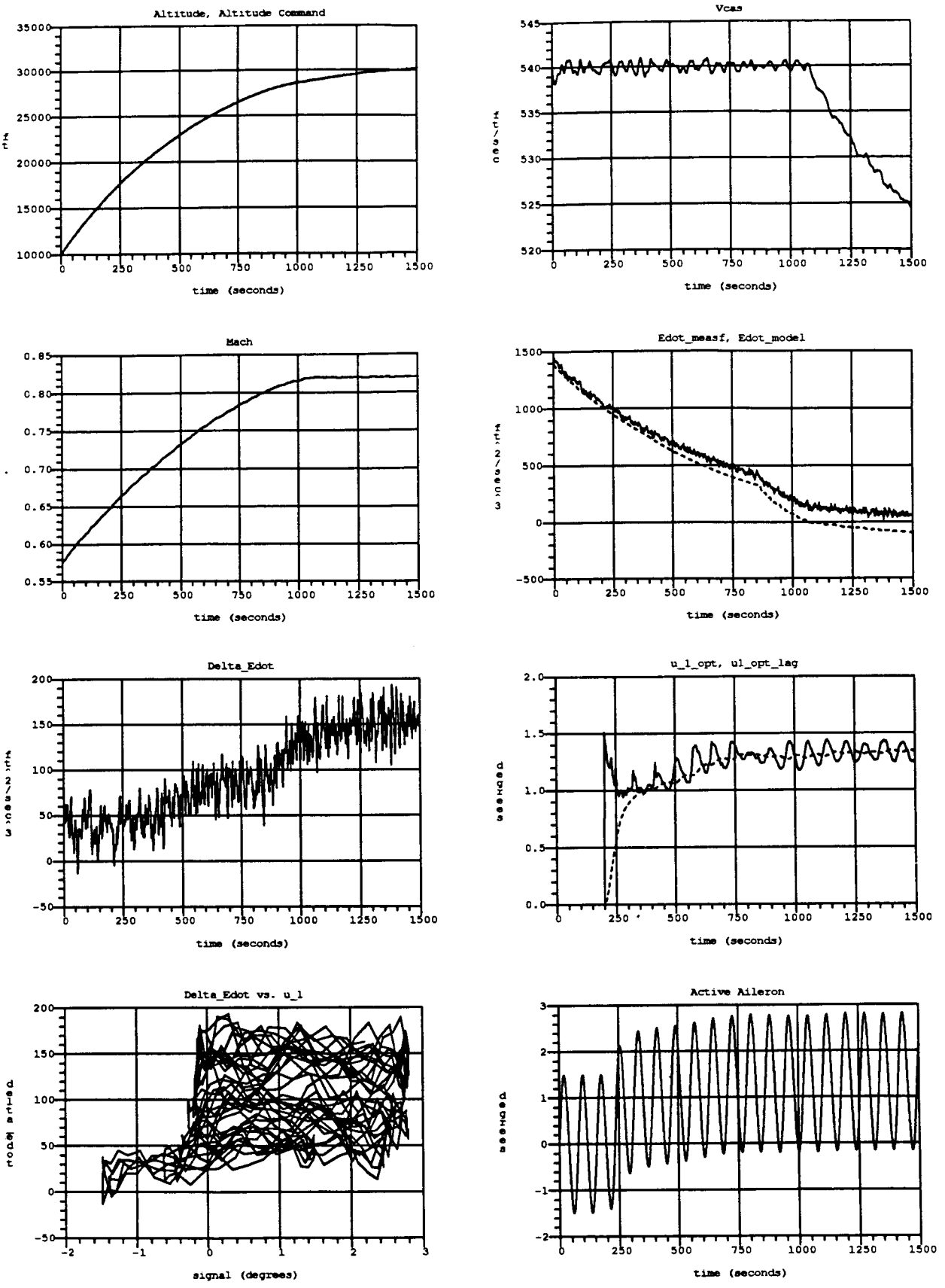

Figure A.8: Optimization During Climb, Light Disturbance

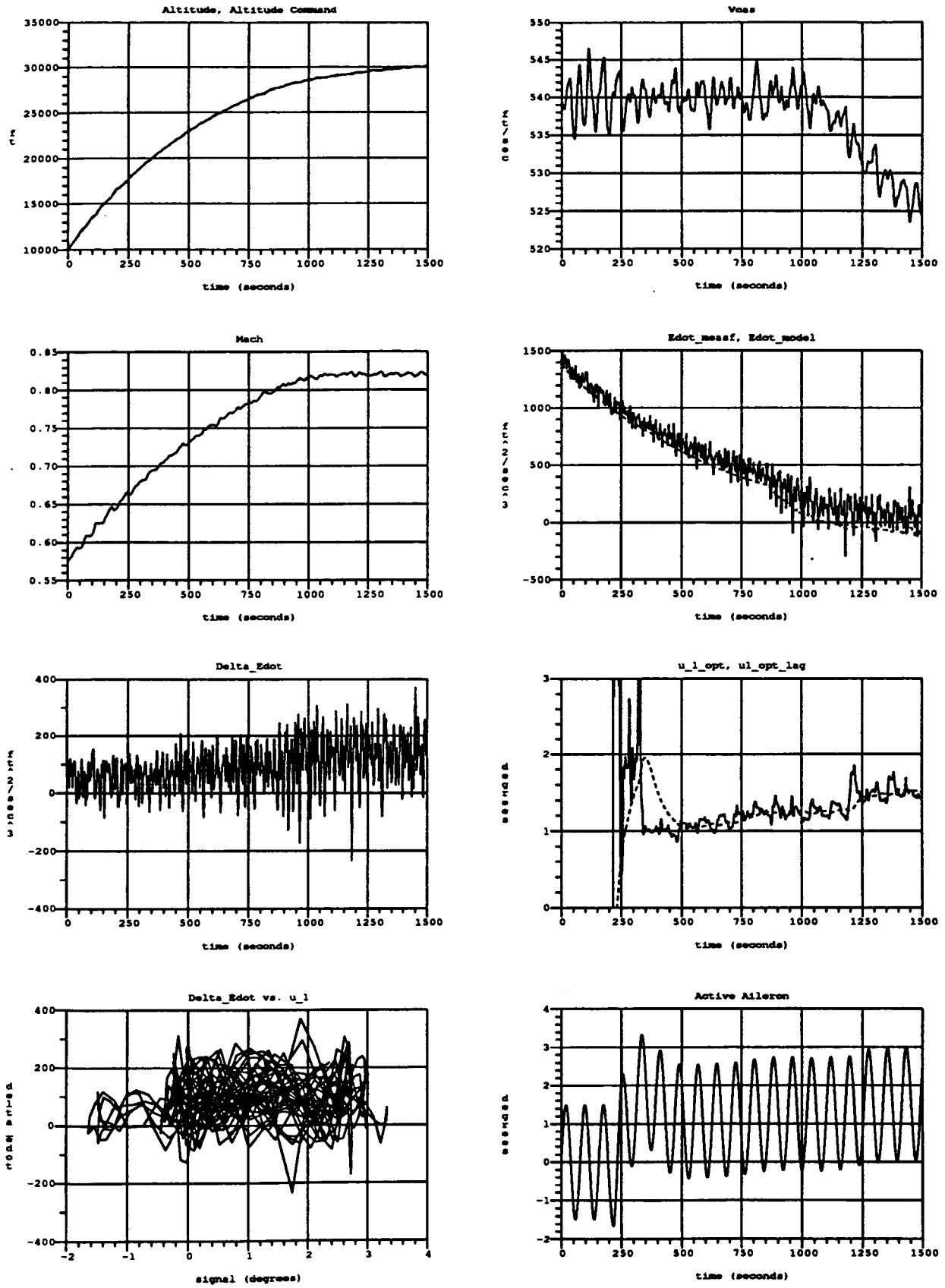

Figure A.9: Optimization During Climb, Moderate Disturbance

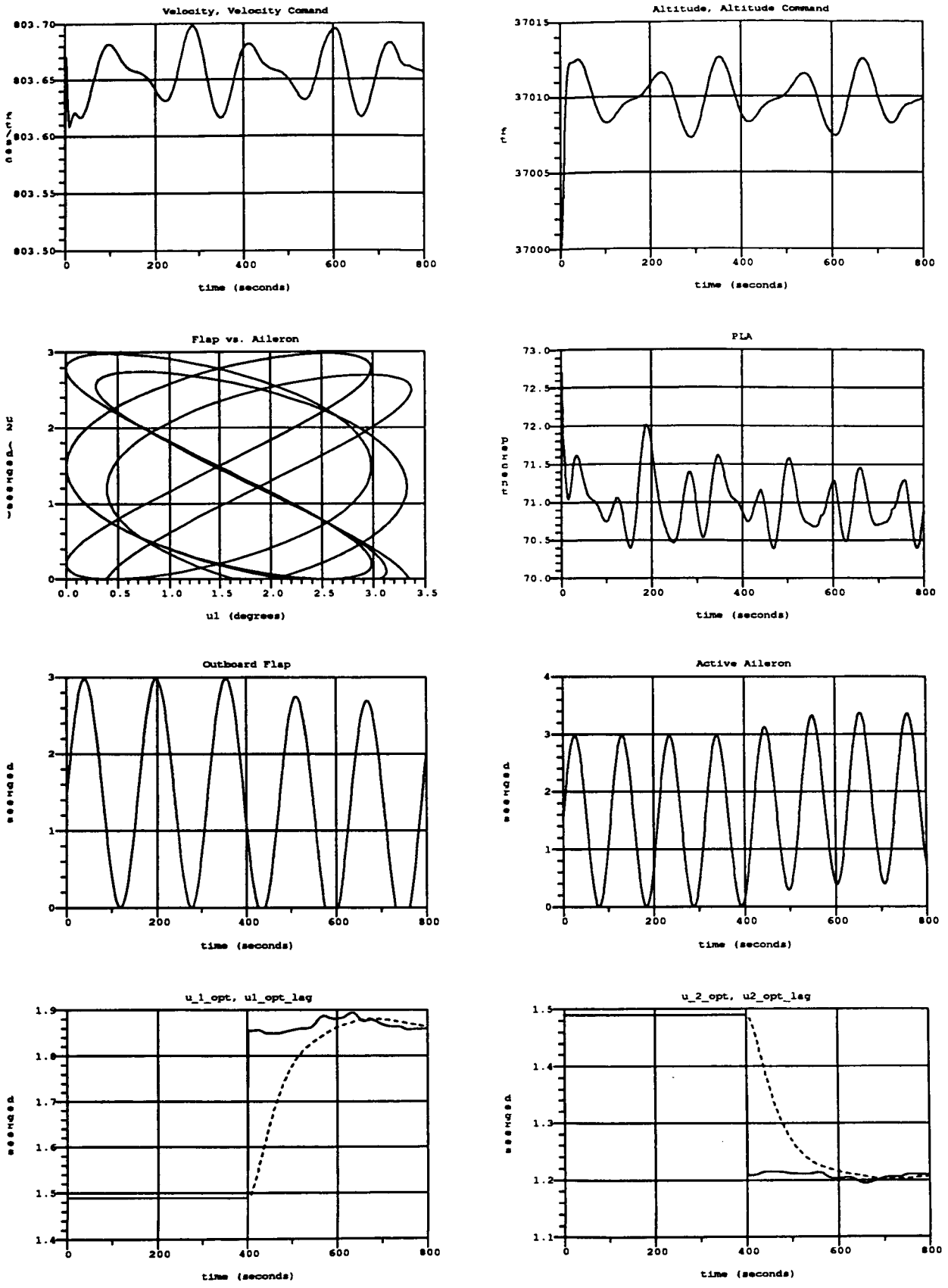

Figure A.10: Optimization of Multiple Effectors, No Disturbance

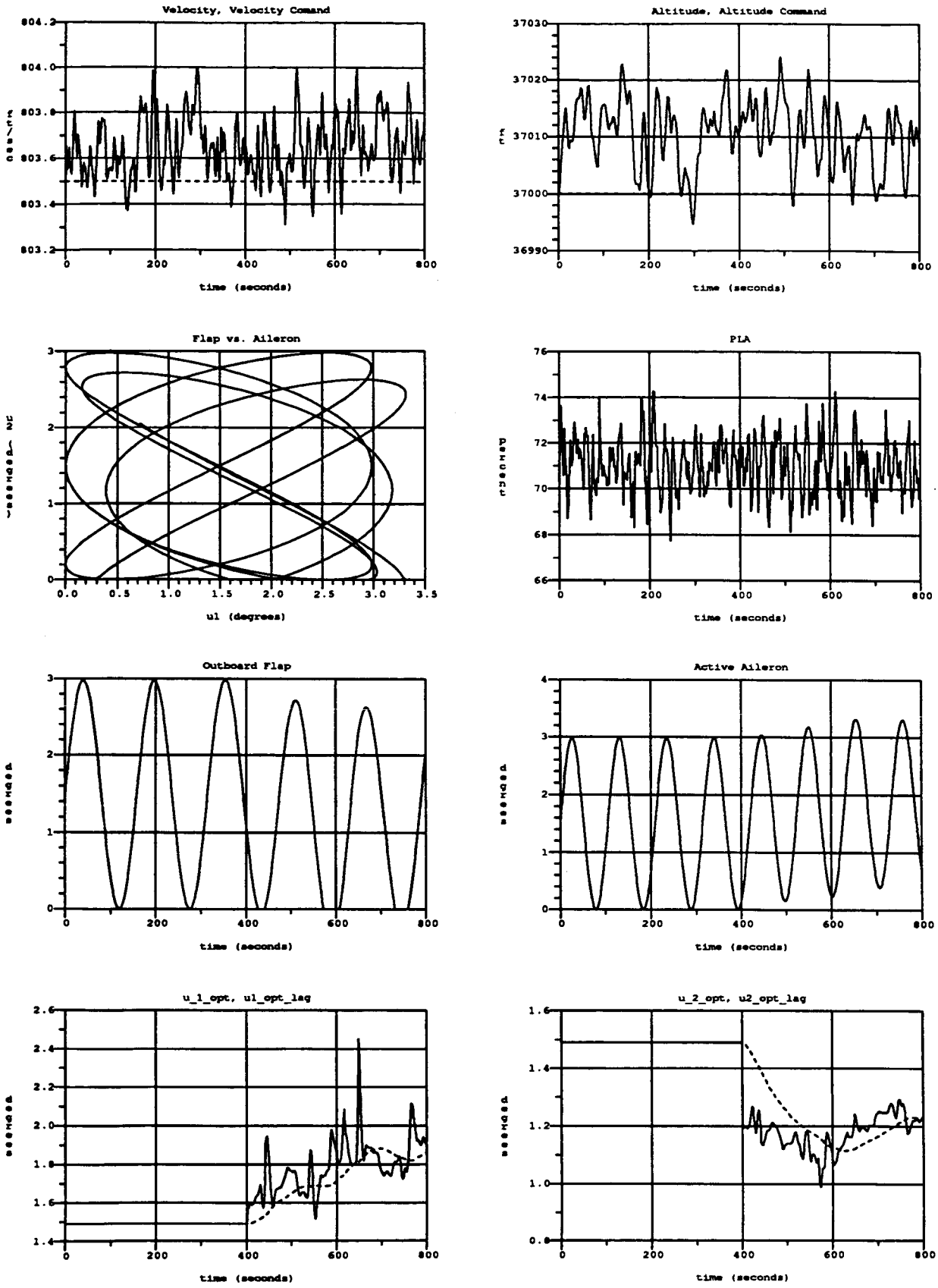

Figure A.11: Optimization of Multiple Effectors, Light Disturbance

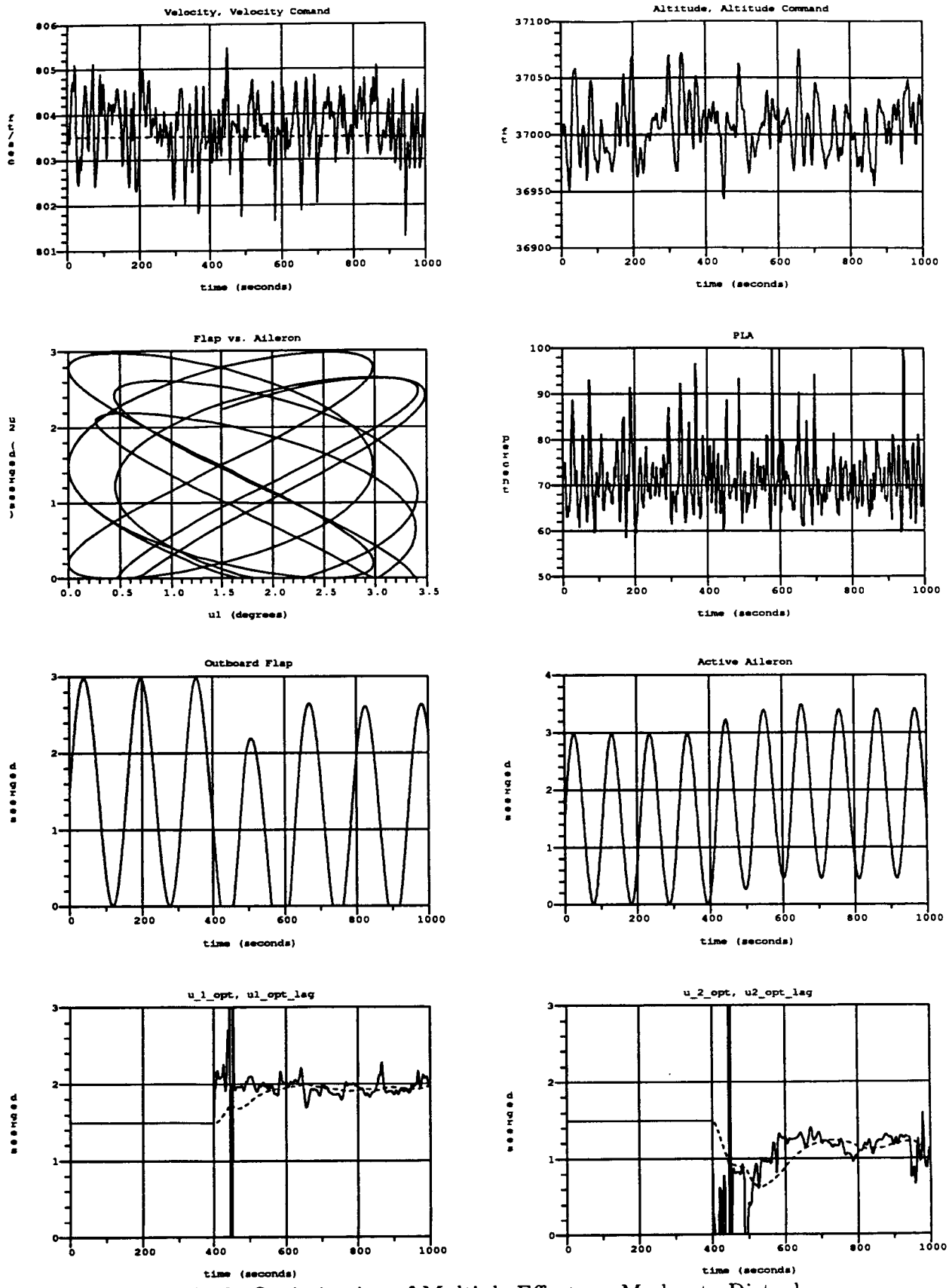

Figure A.12: Optimization of Multiple Effectors, Moderate Disturbance

Appendix B

Analytical Optimization

For the special aerodynamic model given in Section 2.2, it is possible to analytically derive the optimal surface positions. It is also possible to use these results to compute the variation of the optimal surface positions with respect to the lift coefficient. This result can be used to compute values for the feedforward decoupling gains P_1 and P_2 referenced in Section 3.4.

The analysis is shown below for both the active ailerons and the outboard flaps. Optimization of just the active ailerons is a special case of the general solution and will be shown later.

Consider the special aerodynamic model given in Section 2.2:

$$\begin{aligned} C_D &= C_{D_1} + C_{D_2}\alpha + C_{D_3}\delta_{ht} + C_{D_4}\delta_{aa} + C_{D_5}\delta_{fl} + C_{D_6}\alpha^2 + C_{D_7}\delta_{ht}^2 + C_{D_8}\delta_{aa}^2 + \\ &\qquad C_{D_9}\delta_{fl}^2 + C_{D_{10}}\alpha\delta_{ht} + C_{D_{11}}\alpha\delta_{aa} + C_{D_{12}}\alpha\delta_{fl} \\ C_L &= C_{L_o} + C_{L_\alpha}\alpha + C_{L_{ht}}\delta_{ht} + C_{L_{aa}}\delta_{aa} + C_{L_{fl}}\delta_{fl} + C_{L_q}\frac{q\bar{c}}{2V_t} \\ C_M &= C_{M_o} + C_{M_\alpha}\alpha + C_{M_{ht}}\delta_{ht} + C_{M_{aa}}\delta_{aa} + C_{M_{fl}}\delta_{fl} + C_{M_q}\frac{q\bar{c}}{2V_t} \end{aligned}$$

The objective of the analytical optimization is to minimize the drag at steady level flight.

$$\min_{\alpha,\delta_{ht},\delta_{aa},\delta_{fl}} C_D \qquad \text{subject to : } C_L = C_{L_{spec}}\ ,\ C_M = 0$$

where $C_{L_{spec}}$ is the lift coefficient required to achieve steady level flight at the desired flight condition.

This optimization can be computed by considering a cost function that represents the drag

coefficient adjoined with the constraint equations.

$$J = C_D + \lambda_L(C_L - C_{L_{spec}}) + \lambda_M C_M$$

At the optimal value of the surface positions, the variation of the cost function will be zero for arbitrary variations of the independent variables.

$$\begin{aligned}
\delta J \;=\; & C_{D_2}\delta\alpha + C_{D_3}\delta\delta_{ht} + C_{D_4}\delta\delta_{aa} + C_{D_5}\delta\delta_{fl} + 2C_{D_6}\alpha\,\delta\alpha + 2C_{D_7}\delta_{ht}\,\delta\delta_{ht} \\
& + 2C_{D_8}\delta_{aa}\,\delta\delta_{aa} + 2C_{D_9}\delta_{fl}\,\delta\delta_{fl} + (C_{D_{10}}\delta_{ht} + C_{D_{11}}\delta_{aa} + C_{D_{12}}\delta_{fl})\delta\alpha \\
& + C_{D_{10}}\alpha\,\delta\delta_{ht} + C_{D_{11}}\alpha\,\delta\delta_{aa} + C_{D_{12}}\alpha\,\delta\delta_{fl} \\
& + \delta\lambda_L(C_{L_o} + C_{L_\alpha}\alpha + C_{L_{ht}}\delta_{ht} + C_{L_{aa}}\delta_{aa} + C_{L_{fl}}\delta_{fl} - C_{L_{spec}}) \\
& + \lambda_L(C_{L_\alpha}\delta\alpha + C_{L_{ht}}\delta\delta_{ht} + C_{L_{aa}}\delta\delta_{aa} + C_{L_{fl}}\delta\delta_{fl}) \\
& + \delta\lambda_M(C_{M_o} + C_{M_\alpha}\alpha + C_{M_{ht}}\delta_{ht} + C_{M_{aa}}\delta_{aa} + C_{M_{fl}}\delta_{fl} - C_{M_{spec}}) \\
& + \lambda_M(C_{M_\alpha}\delta\alpha + C_{M_{ht}}\delta\delta_{ht} + C_{M_{aa}}\delta\delta_{aa} + C_{M_{fl}}\delta\delta_{fl}) = 0
\end{aligned}$$

Collecting terms:

$$\begin{aligned}
\delta J \;=\; & (C_{D_2} + 2C_{D_6}\alpha + C_{D_{10}}\delta_{ht} + C_{D_{11}}\delta_{aa} + C_{D_{12}}\delta_{fl} + \lambda_L C_{L_\alpha} + \lambda_M C_{M_\alpha})\delta\alpha \\
& + (C_{D_3} + 2C_{D_7}\delta_{ht} + C_{D_{10}}\alpha + \lambda_L C_{L_{ht}} + \lambda_M C_{M_{ht}})\delta\delta_{ht} \\
& + (C_{D_4} + 2C_{D_8}\delta_{aa} + C_{D_{11}}\alpha + \lambda_L C_{L_{aa}} + \lambda_M C_{M_{aa}})\delta\delta_{aa} \\
& + (C_{D_5} + 2C_{D_9}\delta_{fl} + C_{D_{12}}\alpha + \lambda_L C_{L_{fl}} + \lambda_M C_{M_{fl}})\delta\delta_{fl} \\
& + (C_{L_o} + C_{L_\alpha}\alpha + C_{L_{ht}}\delta_{ht} + C_{L_{aa}}\delta_{aa} + C_{L_{fl}}\delta_{fl} - C_{L_{spec}})\delta\lambda_L \\
& + (C_{M_o} + C_{M_\alpha}\alpha + C_{M_{ht}}\delta_{ht} + C_{M_{aa}}\delta_{aa} + C_{M_{fl}}\delta_{fl} - C_{M_{spec}})\delta\lambda_M = 0
\end{aligned}$$

All of the above parenthetical expressions must be zero to allow arbitrary variation of the independent variables and still achieve zero total variation of the cost function. Expressing these equations in matrix form:

$$\begin{bmatrix}
2C_{D_6} & C_{D_{10}} & C_{D_{11}} & C_{D_{12}} & C_{L_\alpha} & C_{M_\alpha} \\
C_{D_{10}} & 2C_{D_7} & 0 & 0 & C_{L_{ht}} & C_{M_{ht}} \\
C_{D_{11}} & 0 & 2C_{D_8} & 0 & C_{L_{aa}} & C_{M_{aa}} \\
C_{D_{12}} & 0 & 0 & 2C_{D_9} & C_{L_{fl}} & C_{M_{fl}} \\
C_{L_\alpha} & C_{L_{ht}} & C_{L_{aa}} & C_{L_{fl}} & 0 & 0 \\
C_{M_\alpha} & C_{M_{ht}} & C_{M_{aa}} & C_{M_{fl}} & 0 & 0
\end{bmatrix}
\begin{bmatrix} \alpha \\ \delta_{ht} \\ \delta_{aa} \\ \delta_{fl} \\ \lambda_L \\ \lambda_M \end{bmatrix}
=
\begin{bmatrix} -C_{D_2} \\ -C_{D_3} \\ -C_{D_4} \\ -C_{D_5} \\ C_{L_{spec}} - C_{L_o} \\ -C_{M_o} \end{bmatrix}$$

This equation can be solved numerically for a given flight condition. For the case of just active ailerons without the outboard flaps, the result can be expressed by the following equation:

$$\begin{bmatrix}
2C_{D_6} & C_{D_{10}} & C_{D_{11}} & C_{L_\alpha} & C_{M_\alpha} \\
C_{D_{10}} & 2C_{D_7} & 0 & C_{L_{ht}} & C_{M_{ht}} \\
C_{D_{11}} & 0 & 2C_{D_8} & C_{L_{aa}} & C_{M_{aa}} \\
C_{L_\alpha} & C_{L_{ht}} & C_{L_{aa}} & 0 & 0 \\
C_{M_\alpha} & C_{M_{ht}} & C_{M_{aa}} & 0 & 0
\end{bmatrix}
\begin{bmatrix} \alpha \\ \delta_{ht} \\ \delta_{aa} \\ \lambda_L \\ \lambda_M \end{bmatrix}
=
\begin{bmatrix} -C_{D_2} \\ -C_{D_3} \\ -C_{D_4} \\ C_{L_{spec}} - C_{L_o} \\ -C_{M_o} \end{bmatrix}$$

For the flight condition used for the steady level simulations in this report, 37,000 feet, Mach 0.827, the following aerodynamic coefficients are applicable:

$$
\begin{aligned}
C_{D_1} &= .01736 \\
C_{D_2} &= -.1282 \\
C_{D_3} &= -.03168 \\
C_{D_4} &= -0.01711 \\
C_{D_5} &= -.02298 \\
C_{D_6} &= 7.748 \\
C_{D_7} &= .3062 \\
C_{D_8} &= .3281 \\
C_{D_9} &= .6598 \\
C_{D_{10}} &= 3.510 \\
C_{D_{11}} &= .1223 \\
C_{D_{12}} &= .1223 \\
C_{L_o} &= .06411 \\
C_{L_\alpha} &= 7.107 \\
C_{L_{ht}} &= 1.503 \\
C_{L_{\alpha\alpha}} &= .1075 \\
C_{L_{fl}} &= .1084 \\
C_{M_o} &= -.09163 \\
C_{M_\alpha} &= -1.409 \\
C_{M_{ht}} &= -3.711 \\
C_{M_{\alpha\alpha}} &= -.1502 \\
C_{M_{fl}} &= -.07821
\end{aligned}
$$

The lift coefficient necessary for level flight is $C_{L_{spec}} = 0.54$. The optimal solution with the outboard flaps included is:

$$
\begin{aligned}
\delta_{\alpha\alpha} &= 1.9003 \text{ degrees} \\
\delta_{fl} &= 1.186 \text{ degrees} \\
\delta_{ht} &= -3.238 \text{ degrees} \\
\alpha &= 4.475 \text{ degrees}
\end{aligned}
$$

The optimal solution with the outboard flaps not included is:

$$
\begin{aligned}
\delta_{\alpha\alpha} &= 1.9036 \text{ degrees} \\
\delta_{ht} &= -3.194 \text{ degrees} \\
\alpha &= 4.483 \text{ degrees}
\end{aligned}
$$

These values compare quite well with the values empirically derived in Section 2.5 by calling the full aerodynamic database, and the values of the control surfaces found by the adaptive controller.

As the lift coefficient varies, the optimal surface positions vary. To compute the variation of the optimal surface positions the optimal solution is numerically differenced by computing the solution at two C_L's (C_{L_1} and C_{L_2}). Representing the relationship between the optimal surface positions as a 3-D line:

$$\begin{bmatrix} \delta_{ht} \\ \delta_{aa} \\ \delta_{fl} \end{bmatrix} = \begin{bmatrix} \delta_{ht_1} \\ \delta_{aa_1} \\ \delta_{fl_1} \end{bmatrix} + c \begin{bmatrix} \delta_{ht_2} - \delta_{ht_1} \\ \delta_{aa_2} - \delta_{aa_1} \\ \delta_{fl_2} - \delta_{fl_1} \end{bmatrix}$$

Normalizing the direction vector for unit δ_{ht} results in the first column of the mixing matrix described in Section 3.4.

$$\begin{bmatrix} 1 \\ P_1 \\ P_2 \end{bmatrix} = \begin{bmatrix} 1 \\ \frac{\delta_{ht_2} - \delta_{ht_1}}{\delta_{aa_2} - \delta_{aa_1}} \\ \frac{\delta_{ht_2} - \delta_{ht_1}}{\delta_{fl_2} - \delta_{fl_1}} \end{bmatrix} = \begin{bmatrix} 1 \\ -0.4010 \\ -0.1915 \end{bmatrix}$$

For the case without the outboard flaps,

$$P_1 = \frac{\delta_{ht_2} - \delta_{ht_1}}{\delta_{aa_2} - \delta_{aa_1}} = -0.4045$$

The simulations performed in this report do not use these values of P_1 and P_2. Several experiments were performed with these values in the mixing matrix and the performance of the adaptive controller was not significantly changed.

Bibliography

[1] Glenn B. Gilyard and Martín España, "On the Use of Controls for Subsonic Transport Performance Improvement: Overview and Future Directions", NASA TM-4605, August 1994.

[2] Thomas Ting, Dale Enns, "Subsonic Transport Adaptive Performance Optimization", Final Report, July 1994

[3] Dale Enns, "Vertical Plane Point Mass Motion of an Airplane", University of Minnesota class notes, 4 April 1994.

[4] Dale Enns, "Vertical Plane Rigid Body Motion of an Airplane", University of Minnesota class notes, 27 April 1994.

[5] John D. Anderson, "Introduction to Flight, 3rd Edition", McGraw Hill, 1989, ISBN 0-07-001641-0

[6] C.R. Chalk, T.P. Neal, T.M. Harris, F.E. Pritchard, R. J. Woodcock, "Background Information and User Guide for MIL-F-8785B(ASG), 'Military Specification - Flying Qualities of Piloted Airplanes' ", Technical Report AFFDL-TR-69-72, August 1969

[7] L. E. Becker, G. E. Hunt, W. J. Leath, "Documentation of the Lockheed L-1011 S/N 1001 Aircraft Simulation", Pub. No. SP710-30, Contract NAS-16072, July 1984

[8] ARINC Characteristic 704-3 for Inertial Reference Systems, prepared by Airlines Electronic Engineering Committee, March 13, 1981.

[9] Bugajski, D.J., Enns, D.F., Hendrick, R.C., "Multi-Application Control (MACH), HARV Reports," Honeywell Technology Center, 8 November 1994.

[10] Enns, D. F., Bugajski, D.J., Carter, J., Antoniewicz, R., Multi-Application Control," Fourth High Alpha Conference, NASA Dryden Flight Research Center, Edwards, California, July 12-14, 1994.

[11] Honeywell, "Multivariable Control Design Guidelines (First Draft)," U. S. Air Force Contract Number F33615-92-C-3607, 18 May 1995.

[12] Enns, D.F., Bugajski, D.J., Hendrick, R. C., Stein, G., "Dynamic Inversion: An Evolving Methodology For Flight Control Design," International Journal of Control, Volume 59, Number 1, pages 71-91, 1994.

[13] "Advanced Fighter Technology Integration F-111 Mission Adaptive Wing", NASA CP-3055, proceedings of a symposium held at NASA Ames Center Dryden Flight Research Facility, Edwards, California, Apr. 4-6, 1989. (ITAR restricted document)

[14] Martín España and Glenn Gilyard, "Direct Adaptive Performance Optimization of Subsonic Transports: A Periodic Perturbation Technique", NASA TM-4676, March 1995.

[15] Sorensen, John A, et.al., "Application of Trajectory Optimization Principles to Minimize Aircraft Operating Costs", IEEE TA3-9:00, 1979,

[16] Erzberger, Heinz, "Automation of On-Board Flightpath Management", NASA TM-84212, December 1981.

[17] Visser, H. G., "An Approach to On-Board Optimization of Cruise at Constant Altitude", Delft Technische Univiversity, Report No. LR-581, 1989.

REPORT DOCUMENTATION PAGE

Form Approved
OMB No. 0704-0188

1. AGENCY USE ONLY (Leave blank)	2. REPORT DATE	3. REPORT TYPE AND DATES COVERED
	September 1995	Contractor Report—Feb. 14–Jul. 14, 1995

4. TITLE AND SUBTITLE

A Concept for Adaptive Performance Optimization on Commercial Transport Aircraft

5. FUNDING NUMBERS

WU 505-69-10

6. AUTHOR(S)

Michael R. Jackson and Dale F. Enns

7. PERFORMING ORGANIZATION NAME(S) AND ADDRESS(ES)

Honeywell Technology Center
3660 Technology Drive
Minneapolis, MN 55418

8. PERFORMING ORGANIZATION REPORT NUMBER

Honeywell contract
F 5069

9. SPONSORING/MONOTORING AGENCY NAME(S) AND ADDRESS(ES)

National Aeronautics and Space Administration
Dryden Flight Research Center
P.O. Box 273
Edwards, CA 93523-0273

10. SPONSORING/MONITORING AGENCY REPORT NUMBER

NASA CR-186034
(H-2072)

11. SUPPLEMENTARY NOTES

Dryden Technical Monitor: Glenn B. Gilyard, NASA contract NAS4-50021, Advanced Concepts for Aeronautics.

12a. DISTRIBUTION/AVAILABILITY STATEMENT

Unclassified—Unlimited
Subject Categories 02 and 03

12b. DISTRIBUTION CODE

13. ABSTRACT (Maximum 200 words)

An adaptive control method is presented for the minimization of drag during flight for transport aircraft. The minimization of drag is achieved by taking advantage of the redundant control capability available in the pitch axis, with the horizontal tail used as the primary surface and symmetric deflection of the ailerons and cruise flaps used as additional controls. The additional control surfaces are excited with sinusoidal signals, while the altitude and velocity loops are closed with guidance and control laws. A model of the throttle response as a function of the additional control surfaces is formulated and the parameters in the model are estimated from the sensor measurements using a least squares estimation method. The estimated model is used to determine the minimum drag positions of the control surfaces. The method is presented for the optimization of one and two additional control surfaces. The adaptive control method is extended to optimize rate of climb with the throttle fixed. Simulations that include realistic disturbances are presented, as well as the results of a Monte Carlo simulation analysis that shows the effects of changing the disturbance environment and the excitation signal parameters.

14. SUBJECT TERMS

Adaptive control; Aircraft performance; Cambered wings; Drag reduction; Fuel consumption; Optimization

15. NUMBER OF PAGES

68

16. PRICE CODE

AO4

17. SECURITY CLASSIFICATION OF REPORT	18. SECURITY CLASSIFICATION OF THIS PAGE	19. SECURITY CLASSIFICATION OF ABSTRACT	20. LIMITATION OF ABSTRACT
Unclassified	Unclassified	Unclassified	Unlimited